Reliability Assessment of Power Systems Integrated with High-Penetration of Power Converters

by

Bowen Zhang

A dissertation submitted in partial fulfillment
of the requirements for the degree of
Doctor of Philosophy
(Electrical and Computer Engineering)
in the University of Michigan-Dearborn
2022

Doctoral Committee:

Associate Professor Wencong Su, Co-Chair
Associate Professor Mengqi Wang, Co-Chair
Assistant Professor Junho Hong
Assistant Professor Zhen Hu
Associate Professor Taehyung Kim

DEDICATION

This edition of the Ph.D. final dissertation written report by Bowen Zhang, “RELIABILITY ASSESSMENT OF POWER SYSTEMS INTEGRATED WITH HIGH-PENETRATION OF POWER CONVERTERS”, is dedicated to all the professionals, students and people who are working on or interested in power electronic, power system reliability, renewable energy, and complex network information entropy theory.

ACKNOWLEDGEMENTS

Foremost, I would like to express my deepest gratitude and appreciation to my advisor & co-advisor: Prof. Mengqi Wang & Prof. Wencong Su, for their continuous support and insightful guidance through all years of my PhD study. They have encouraged me in all the time of my academic research and daily life, with invaluable advice and plentiful patience.

For willing to be one of my PhD dissertation committee members and provide various suggestions on my academic research, I want to thank Prof. Taehyung Kim, Prof. Junho Hong, and Prof. Zhen Hu. I would also like to thank all my colleagues and friends for a cherished time spent together in the lab and life. I do not have enough space here to list you all, but without a doubt, their kind help and opinions have made my study and life a wonderful time.

Last but not the least, my appreciation goes out to my family. To my parents, Liwu Zhang and Yili Huang. Their support has been unconditional all these years. I am forever grateful for their patience and understanding.

TABLE OF CONTENTS

DEDICATION ..... **ii**

ACKNOWLEDGEMENTS ..... **iii**

LIST OF FIGURES ..... **vii**

LIST OF TABLES ..... **ix**

ABSTRACT ..... **x**

CHAPTER 1: Introduction 1

1.1. Background 1

1.2. Research Objectives 2

1.3. Organization 2

CHAPTER 2: A Three-layer Framework to Assess System Reliability 4

2.1. Introduction 4

2.2. Reliability Concepts 10

2.3. Converter Reliability Formulation 12

2.3.1. Reliability Model of WT Converters 13

2.3.2. Reliability Model of PV Converters 17

2.4. System Level Non-sequential Sampling and Overview 19

2.5. Reliability Mapping Through ML Regression Techniques 21

2.5.1. Theory 22

2.5.2. Support Vector Regression 24

2.5.3. Random Forests 24
2.6. Numerical Analysis 25
2.6.1. System Description 26
2.6.2. Importance of Considering Converter Reliability 27
2.6.3. The Reliability Effect of Converter Topologies 28
2.6.4. The Regression Mapping between Two Levels 30
2.7. Conclusions 31
2.8. References 32
CHAPTER 3: Reliability Ranking and Quantification of Multiple Power Converters 36
3.1. Introduction 36
3.2. Formulation of Converter Reliability 41
3.3. Applying ML Algorithms for Reliability Mapping 44
3.4. Variance-based Global Sensitivity Analysis 47
3.4.1. Theoretical Background 48
3.4.2. Sensitivity Indices 49
3.5. Numerical Analysis 50
3.5.1. The Modified 24-bus IEEE RTS 51
3.5.2. The Reliability Mapping between Two Stages 52
3.5.3. Variance-based GSA Results and Maintenance Suggestions 53
3.6. Conclusions 57
3.7. References 58
CHAPTER 4: Node Reliability Interdependencies and Causal Relation Investigation 61
4.1. Introduction 61

4.2. Transfer Entropy-integrated BN Structure Learning 66
4.2.1. BN Structure Learning 66
4.2.2. Search & Score Functions 67
4.2.3. Transfer Entropy 68
4.2.4. Transfer Entropy-integrated Scoring Function 70
4.3. An Overview of the Proposed Framework 71
4.4. Numerical Analysis 74
4.4.1. Information about the System Physical Network 75
4.4.2. BN Structure Learning Results 75
4.4.3. Outages on Critical Nodes and Their Propagation Areas 80
4.5. Conclusions 82
4.6. References 83
CHAPTER 5: Conclusions and Future Works 86

LIST OF FIGURES

Figure 1. A prediction of the future power system structure.....5

Figure 2. The proposed hierarchical power system reliability assessment framework 8

Figure 3. Typical wind power system 13

Figure 4. PV system with dc-dc boost converter and dc-ac inverter 17

Figure 5. The flowchart of the proposed power system reliability assessment 20

Figure 6. The illustration of RES/power converter penetration in the RTS network.....25

Figure 7. Accumulated EENS of all three scenarios.....28

Figure 8. Scenario II EENS under three converter topologies.....29

Figure 9. Comparison of the predicted and the actual EENS 30

Figure 10. Six steps of the proposed two-stage reliability assessment framework 39

Figure 11. The modified 24-bus IEEE RTS with RES and power converter penetration.....51

Figure 12. Comparison between the predicted and actual EENS 52

Figure 13. First-order indices of PV/WT converter uncertainties 55

Figure 14. Total-effect indices of PV/WT converter uncertainties 55

Figure 15. An overview of the proposed reliability evaluation framework.....65

Figure 16. An overview of the proposed framework 73

Figure 17. The modified 24-bus IEEE RTS network.....74

Figure 18. Calculated entropy values of each variable 76

Figure 19. An example of determining the edge orientation 77

Figure 20. The learned BN structure based on the proposed scoring function.....78

Figure 21. Illustrated critical nodes in the BN structure.....79

Figure 22. Calculated Shannon and transfer entropy (TE) on critical nodes.....79

Figure 23. The failure propagation area when outage happened on node 1 and 13.....81

Figure 24. The failure propagation area when outage happened on node 14 and 15.....82

LIST OF TABLES

Table 1: Reliability indicator under all scenarios 27

Table 2: Total number of devices used in different converter topologies 29

Table 3: ML regression results of SVR and RF 30

Table 4: Sensitivity indices of PV converters under different sample sizes 54

Table 5: Bus information of each section 56

Table 6: Total-effect indices for each divided area 57

Table 7: Literature summary of reliability analysis 62

Table 8: Location and capacity information for WT converters 75

Table 9: Location and capacity information for PV converters 75

Table 10: Location and capacity information for RFPV converters 75

Table 11: Learning comparisons among different scoring functions 77

ABSTRACT

Moving towards renewable and environmental-friendly energy resources has intensified the importance of power electronic converters in future power systems. The issue of reliability becomes more critical than ever before. This research proposes a hierarchical reliability framework to evaluate the electric power system reliability from the power electronic converter level to the overall system level. In the first stage, the reliability of each power converter is modeled in an accurate manner. Dynamic behaviors of various integrated semiconductor devices and the converter topology are considered. In the second stage, we calculate system-level reliability indicators such as expected energy not served (EENS) and loss of load expectation (LOLE) are estimated through a non-sequential Monte Carlo simulation. Machine learning regression models such as support vector regression (SVR) and random forests (RF) are implemented to bridge the nonlinear reliability relationship between two stages. Moreover, a variance-based global sensitivity analysis (GSA) is conducted to rank and identify the most influential converter uncertainties with respect to the variance of system EENS. Based on the GSA conclusions, system operators can take proactive actions to mitigate the potential risk of the system. Furthermore, Bayesian network (BN) structure learning and scoring algorithms are applied to visualize a converter-based BN structure. Reliability interdependencies among different nodes are quantified through information entropy theory such that reliability causal relations can be revealed. This dissertation also studies and discusses opportunities of various emerging technologies. Some improvements and suggestions of the proposed framework are included as well.

CHAPTER 1

Introduction

1.1. Background

The incorporation of renewable energy resources (RES) including solar photovoltaic (PV) generators, wind turbines (WTs) and combined heat and power units (CHPs), have been more favorable, compared to traditional centralized controlled power systems. However, utilizing the power generated from RESs has brought several challenges to realizing a reliable power delivery. That said, the proliferation of RES has been significantly accompanied by the penetration of various power electronic converters. Notably, the power electronic converter plays a fundamental role during energy conversion. Consequently, from a reliability point of view, the system has become more complicated compared with a traditional system.

Meanwhile, various uncertain parameters are introduced in power systems due to intermittent RESs and the operational structure. These uncertainties may have a significant influence on the system's reliability performance. Implementing an appropriate SA on the proposed reliability framework is essential in order to interpret the system reliability behavior and identify the effects that emerging power converters will have on system reliability. Identifying the most critical uncertainties, i.e., the most influential pair of a RES and its connected power converter on the system reliability, will help system operators and stakeholders to better arrange the maintenance schedule and facilitate better system operation.

1.2. Research Objectives

In terms of reliability assessment, power electronic interfaces, namely power converters, play an increasingly important role in recent years with their foreseeable penetration in modern power systems. The main purpose of this research is to evaluate the reliability in a power system while considering the reliability impact from power electronic converters. We bridge the gap between converter and system level reliability and conduct several quantitative analyses with various indices for improving system operation and future planning.

Moreover, the proposed framework presents for the first time the application of the variance-based GSA to identify the contribution of each converter uncertainty to the variance of the system reliability indicator. This novel application is also intended to promote the development of the implementation of more advanced SA methods in power systems so that interested researchers can further interpret the system reliability behavior.

Another purpose of this research is to graphically reveal the reliability inter-dependencies between two power converters through Bayesian Network. Moreover, Information Entropy theory is applied to quantify the uncertainty of each converter and each node. The information or uncertainty transferred from a converter failure event to system reliability performance is also estimated.

1.3. Organization

The Introduction about the Ph.D. dissertation written report was presented in chapter 1. Chapter 2 presents a hierarchical reliability framework to evaluate the electric power system reliability from the power converter level to the overall system level. Chapter 3 introduces a variance-based sensitivity analysis to rank and identify the most influential converter uncertainties

with respect to the variance of system EENS. Chapter 4 presents the investigation of reliability interdependencies among different nodes where each reliability causal relation is quantified with entropy indicators. Chapter 5 summarizes conclusions and future works.

CHAPTER 2

A Three-layer Framework to Assess System Reliability

2.1. Introduction

In recent years, modern power system structures deployed with local available renewable energy resources (RESs), including solar photovoltaic (PV) generators, wind turbines (WTs), and combined heat and power units (CHPs), have been more favorable, compared to traditional centralized controlled power systems. Utilizing the power generated from RESs can reduce the carbon emissions in the environment and significantly increase system operation flexibility [1]. As illustrated in Fig. 1, it is foreseeable that conventional generators will be replaced by different RESs in the future and RESs with smaller capacity, such as rooftop PVs will be widely implemented. As a result, however, the entire system reliability will become more complicated. Specifically, more power conversions will be inevitably required between different energy levels. Whether the generated power from RESs can be efficiently, desirably, and reliably converted to the load side is greatly dependent on the performance of the connected power electronic interfaces. The penetration of power electronic converters has brought a huge challenge to the existing power system structure from a reliability point of view.

The main purpose of conducting reliability evaluation in power systems is to provide quantitative analysis with various indices for improving system operation and future planning [2]. Different methods have been applied for power system reliability evaluation. Analytical methods, such as fault tree analysis (FTA) [3] have been utilized for optimal transmission

system planning. The authors in [4] proposed a system evaluation method based on the minimum path and calculated the reliability indicator on various load points. Simulation methods, such as the Monte Carlo method, have been used [5] to sample the component states in a power system. In [6], an artificial neural network (ANN) was implemented to predict the future reliability of a distribution system through historical data.

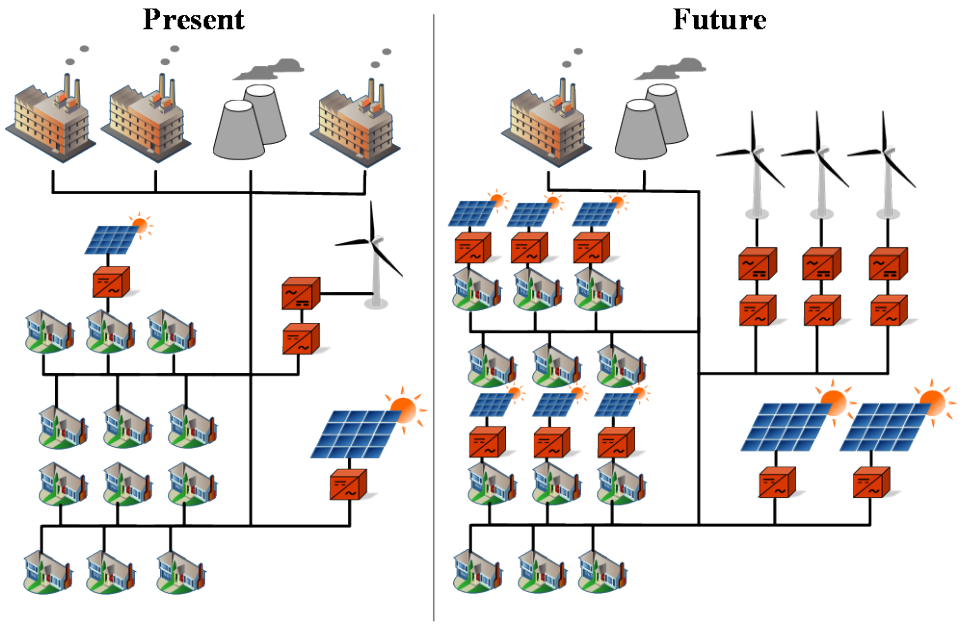

Figure 1. A prediction of the future power system structure

Many of the aforementioned methods have been refined to accommodate the RES contingencies and diverse load demands in power systems. However, failures caused by power converters connected to RESs have been mostly considered as constant or even ignored in most published research works. Authors in [7] investigated the age-related failure of power transformers and assumed 100% reliable for other units. In [8], the authors proposed time-varying reliability models for generating units under high penetration of wind power but didn't consider the potential failure of those connected converters. A reliability assessment was conducted in [9] for components in large scale PV systems, and the inverter failure rate was a constant throughout a

year. In addition, the reliability evaluation of power systems is also dependent on various defined indicators. In addition, the reliability evaluation of power systems is also dependent on various defined indicators. Classic system reliability indices, such as expected energy not supplied (EENS) and loss of load expectation (LOLE), have been widely used for system reliability evaluation [9]. In [11], a series of novel metrics is proposed to understand system reliability performance from various perspectives, including resiliency and power planning. Meanwhile, reliability metrics related to power electronic interfaces, such as semiconductor failure rates and converters' overall power availability have not generated much attention.

That said, researchers in the power electronics field, have concentrated on evaluating the reliability model from both the semiconductor device level and the overall converter level for years. The paper [12] provided a comprehensive review on the reliability issues of semiconductor devices in power converters. Authors in [13]-[14] investigated the reliability of a DC-DC converter where time-to-failure models of semiconductors such as MOSFET and IGBT are included. In [15], the authors presented a reliability comparison among three types of converters used in the grid-connected wind turbines. Meanwhile, many papers have investigated power converter reliability performance when a system is connected to uncertain RES supplies [16]-0. In [16]-[17], reliability and cost analyses of a DC-DC boost converter connected to PV panels were conducted. Authors in [18] proposed a back-to-back power converter for wind turbines to improve the system reliability. Considering the thermal loading and lifetime estimation, a reliability evaluation for critical devices under a typical WT converter topology was performed in [19]. In 0, converters connected to a hybrid PV-wind system were evaluated from efficiency and reliability perspectives. To mathematically estimate power converter reliability, several quantitative methodologies were presented in 0-0. In 0, novel or optimized converter designs were proposed to enhance not only

the device but also the RES reliability performance. In summary, many papers mainly focus on whether the power converter can reliably convert the input power to the grid when faced with the fluctuation on the generation side; however, efficient power conversion from RESs can only guarantee that all the available energy from the environment is injected into the power system. Whether the generated power can be successfully delivered, and is sufficient enough to satisfy the load demand, are still questionable.

Based on the above-mentioned surveys, it can be concluded that many research works have investigated reliability from a specific aspect either the power system or the power electronics field. In terms of reliability assessment, power electronic interfaces, namely power converters, play an increasingly important role in recent years with their foreseeable penetration in modern power systems. Thus, the reliability modeling of power converters is essential when evaluating the system reliability. Meanwhile, the failure-related reliability of power converters is greatly dependent on the semiconductor devices. The proposed framework, therefore, builds a library of failure rates for different semiconductor devices, and calculates all converters' reliability considering different converter topologies.

The overall system reliability is greatly dependent on all converters' performance. However, there is a lack of research regarding how the converter level reliability will affect the system reliability, i.e., the reliability relationship between converter and system level. Further, due to the increasing complexity of modern power systems, this reliability impact from converter to system level remains unknown and cannot be analytically solved.

Thus, another purpose is to bridge this gap between two levels by implementing machine learning (ML) regression analysis. It is well known that regression analysis can establish a relationship among input features and output labels 0, so we consider applying this methodology

for two reasons. First, the reliability indicators of the device and system level are all continuous instead of categorized variables. Second, it is certain that the relationship between two levels is nonlinear. Regression modeling has much better capability to build a nonlinear relationship among input/output data compared with using a look-up table 0. Besides, the complexity of input features increases when more power converters are considered in a power system. The regression method can handle adding any parameter as an input feature of the model, such that the modeling scalability and flexibility are greatly improved.

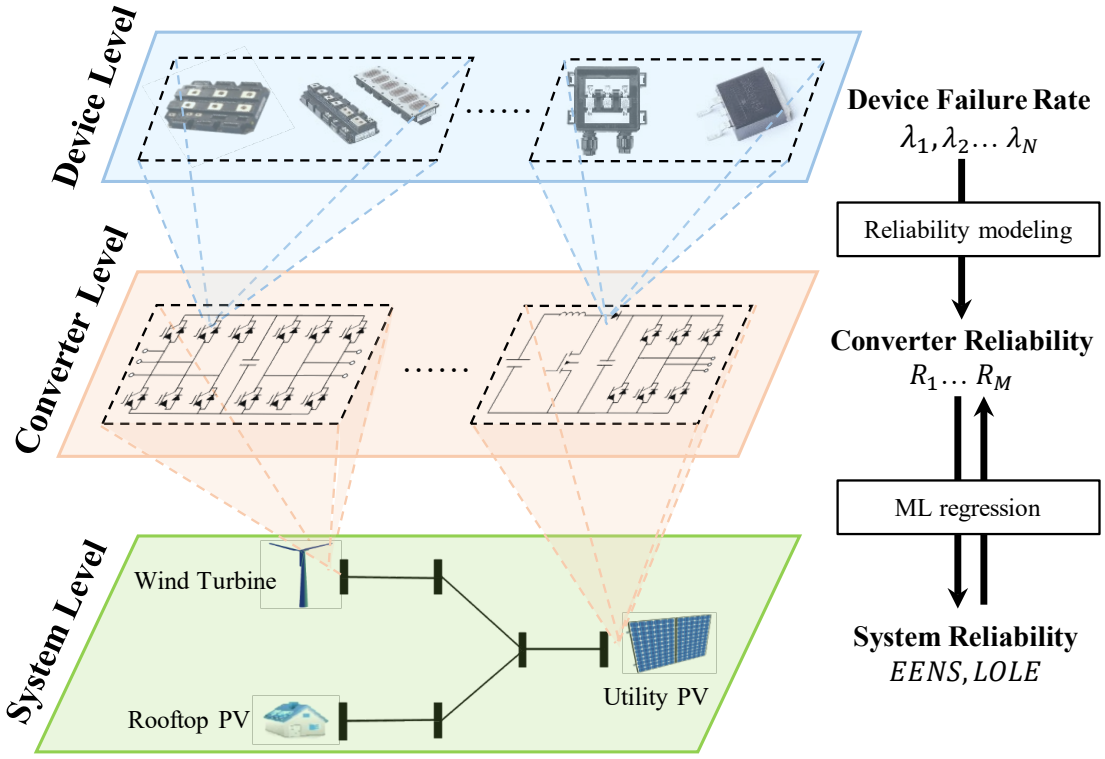

Figure 2. The proposed hierarchical power system reliability assessment framework

In this chapter, we propose a machine learning-based model for the system reliability assessment. As shown in Fig. 2, in the device level, the failure rate model of component is employed under given climate conditions. Several semiconductor devices such as IGBT and diode are included. Then, in the converter level, based on those components' failure rates and converter

topologies, we consider modeling the reliability of different power electronic converters connected to all RESs. After modeling all converters reliability, the system reliability is generated and evaluated by applying system reliability indicators. ML regression techniques are integrated to explore the reliability relationship between converter and system level. This comprehensive procedure is explained in the following sections. The main contributions of this chapter can be summarized as follows.

1) The proposed hierarchical reliability framework consists of three levels. We build a comprehensive library of failure models of a wide range of semiconductor devices, considering their thermal/physical dynamics and environmental conditions. Based on the power converter topology, we apply a combination of device failure rates to build a composite reliability model of each power converter.

2) Due to the proliferation of power converters in a modern power system, their individual reliability indices greatly affect the overall power system performance. Therefore, the ability to generalize the reliability evaluation of converter-dominated power systems is highly valuable and could accelerate the deployment of new power electronics technologies. We present for the first time an integrated three-layer framework to obtain a fundamental understanding of the inter-relationships among device failure rates, power converter reliability, and power system reliability.

A modern power system usually involves a large number of components and sub-systems. A fundamental understanding of the reliability impacts from converter failure to the overall system performance is still an unsolved puzzle. Conventional approaches are reliant on human-expert prior knowledge that may not be quantitative. To collectively solve these challenges, we leverage modern machine learning (ML) techniques to provide a baseline tool that can capture the

dependence structure for a large group of components and evaluate the reliability indices of converter-dominated power system at scale. The knowledge obtained from ML can provide theoretically sound yet easy-to-implement guidelines for power system operators to mitigate eventual failures. It is worth noting that it is not our focus to deliver a commercial-grade ML tool. The goal is, rather, to provide a baseline platform to the research society so that interested users can further study the reliability performance of converter-dominated power systems by incorporating more advanced ML algorithms.

2.2. Reliability Concepts

Reliability is a specific measurement and an inherent characteristic of a device or system which describes its ability to perform its intended function within a period of time [1]. According to this definition, a device/system is considered reliable if its regular performance can be retained during a specified time interval. On the contrary, if failures happen during the interval and the performance cannot meet the pre-defined requirement, the device/system is considered unreliable, and maintenance is required to improve its reliability. To quantitatively measure the reliability of a device or system, different reliability indicators have been developed. Furthermore, if a system is composed of several sub-systems, its reliability evaluation becomes complicated because each sub-system should be evaluated first with corresponding reliability indicators.

An electric power system is a typical complex system that consists of various components and sub-systems. The system function that is, meeting the power demand on all load points should be guaranteed at all times. As a result, classic indices such as EENS and LOLE were developed to evaluate system reliability from energy and load loss perspectives. A system with a high value of EENS/LOLE is considered an unreliable system. For an ideal power system, the power generation is sufficient, and the load demand is satisfied all the time, such that both EENS and LOLE can

reach zero; however, contingencies and failures can happen at any component during any time under a modern power system, resulting in an increase on those indices. Components, including generators, transmission lines, and load points, can fail due to random outages or aging issues.

Moreover, with the development of renewable energy technology, RESs such as WTs and PV systems are replacing traditional diesel generators in today's power systems. Their power generations are largely dependent on time-variant ambient conditions, though, which introduces more uncertainty into power systems and may ultimately affect system reliability. Thus, evaluating the components' reliability is essential when assessing the reliability performance of a power system.

As one of components in a power system, the power electronic converter has not garnered much attention when evaluating system reliability performance. However, accompanied by increasing RES implementation in modern power systems, the power electronic converter is necessarily equipped as an interface to deal with power conversion. The generated power from a WT or PV source can be successfully injected into the grid only if the power converter operates correctly at all times. Thus, the reliability of power converters is of great importance as it may affect the entire system's reliability. In addition, a power converter is composed of various semi-conductor devices. For each of these devices, the device failure rate is usually used as one of the reliability indices to evaluate its reliability. Furthermore, the time-varying operating condition and thermal stress on a device will greatly affect its failure rate. In conclusion, the reliability of a power converter should be modeled based on its critical devices and should be taken into consideration when evaluating power system reliability.

Therefore, with the increased penetration of RESs and power converters in modern power systems, reliability can be modeled hierarchically with two levels. First, the WT/PV converter

reliability modeling is built based on various devices considering thermal effects and operating conditions. The converter topologies are also considered to determine the total number of devices. Then, together with other components' reliability, the converter reliability is incorporated into the system level analysis and the system reliability indices, including EENS and LOLE are estimated. The detailed reliability modeling for the converter level is described in the next section.

2.3. Converter Reliability Formulation

First, the reliability of each power converter connected to a RES (WT or PV system) should be practically quantified. As in equation (2.1), the reliability value *R(t)* is traditionally calculated from the failure rate λ, where λ is independent of time and treated as a constant value [10].

$$R(t) = e^{-\lambda t} \tag{2.1}$$

However, surveys show that the values of failure rates are greatly affected by various factors, including ambient variations and device thermal loading [11]. To consider those factors which have potential reliability impact on a power converter, the general FIDES model is used in this chapter, and expressed in the following equation (2.2) [25], where Π_{PM} is the contribution from quality and technical control over manufacturing of the component. $\Pi_{Process}$ consists of all processes, from specification to field operation and maintenance. These two parameters are assumed to be one in the proposed modeling process.

$$\lambda = \Pi_{PM}\Pi_{Process}\lambda_{Phy} \tag{2.2}$$

λ_{Phy} is of paramount importance in this equation which takes all component states into account, and is calculated by:

$$\lambda_{Phy} = \sum_{i}^{States} \left[\frac{t_{annual}}{T}\right]_i \Pi_i \lambda_i \tag{2.3}$$

where t_{annual} is the duration of the ith state throughout the time span T. Π_i is the induced overstress electrical factor which is defined by the user and are specific to each component 0. λ_i is calculated depended on the specific component and is used to estimate its final component failure rate. The detailed process is presented below.

2.3.1. Reliability Model of WT Converters

A typical wind power system is considered, consisting of a permanent magnet synchronous generator (PMSG), a generator-side inverter, a dc link, and a grid-side inverter, as shown in Fig. 3. The WT output power varies with the wind speed and angle. This results in the variation of device power losses, and ultimately affects the device failure rate. Thus, hourly based wind speed data is collected to determine the output power $P_{wt,t}$ at hour t which is estimated in equation (2.4), where v_t is the wind speed, P_{rated} represents the rated capacity, $v_{ci}, v_r,$ and v_{co} are the cut-in, rated, and cut-out wind speeds of the WT system, respectively. Thus, hourly based wind speed data is collected to determine the output power $P_{wt,t}$ at hour t [26].

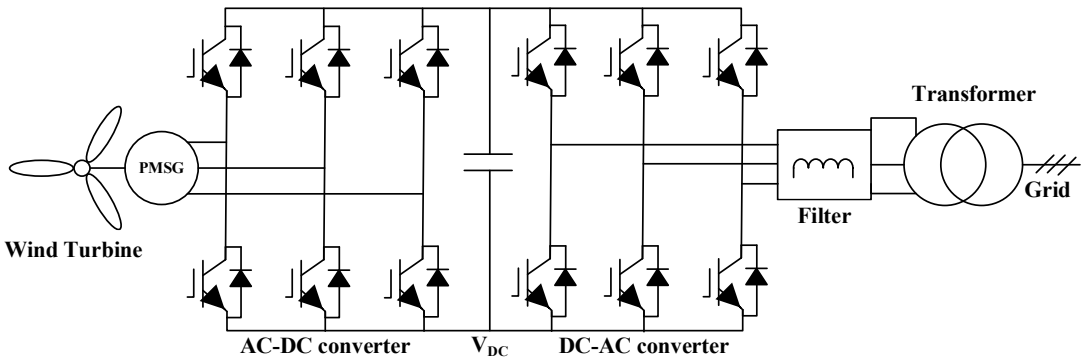

Figure 3. Typical wind power system

$$P_{wt,t} = \begin{cases} 0, & 0 \le v_t \le v_{ci} \\ (A + Bv_t + Cv_t^2)P_{rated}, & v_{ci} \le v_t \le v_r \\ P_{rated}, & v_r \le v_t \le v_{co} \\ 0, & v_t \ge v_{co} \end{cases} \quad (2.4)$$

As shown in equation (2.4), a second-order function is applied to estimate this non-linear function where v_t is the wind speed, P_{rated} represents the rated capacity, v_{ci}, v_r, and v_{co} are the cut-in, rated, and cut-out wind speeds of the WT system, respectively [27].

Then, the power losses of power electronic devices in the WT can be estimated. Critical semiconductors considered here are diodes and IGBTs. The total device power losses consist of conduction loss and switching loss. Both losses are determined by various parameters. For example, the diode/IGBT conduction loss is related to its resistance and voltage drop, while switching loss is related to the switching frequency [19].

$$P_{WT_{IGBT_{con}}} = I_{wt}V_{CEO}\left(\frac{1}{2\pi} + \frac{Mcos\varphi}{8}\right) + {I_{wt}}^2 r_{CE}\left(\frac{1}{8} + \frac{M}{3\pi}cos\varphi\right) \tag{2.5}$$

$$P_{WT_{diode_{con}}} = I_{wt}V_{F0}\left(\frac{1}{2\pi} - \frac{Mcos\varphi}{8}\right) + {I_{wt}}^2 r_F\left(\frac{1}{8} - \frac{M}{3\pi}cos\varphi\right) \tag{2.6}$$

Equations (2.5) and (2.6) express the calculation of the conduction loss of a diode and an IGBT, respectively, where I_{wt} represents the peak phase current and can be calculated from P_{wt}; V_{CEO}, V_{F0} are the threshold voltage drops on the IGBT and diode respectively; r_{CE}, r_F denotes the resistances of the IGBT and diode; M represents the modulation ratio; and φ is the angle between the voltage and current.

$$P_{WT\_IGBT\_sw} = \frac{1}{\pi} f_{sw}(E_{on} + E_{off}) \frac{I_{wt}V_{DC}}{V_{ref\_IGBT}I_{ref\_IGBT}} \tag{2.7}$$

$$P_{WT\_diode\_sw} = \frac{1}{\pi} f_{sw}E_{rec} \frac{I_{wt}V_{DC}}{V_{ref\_diode}I_{ref\_diode}} \tag{2.8}$$

The switching loss can be calculated as in (2.7) and (2.8), where E_{on} and E_{off} are the IGBT energy losses of the ON and OFF state; V_{ref_IGBT} and I_{ref_IGBT} are the reference commutation voltage and current of the IGBT; V_{ref_diode} and I_{ref_diode} are the reference

commutation voltage and current of the diode; and E_{rec} is the rated switching energy loss of the diode.

The total power loss of a diode/IGBT can be derived by adding its conduction loss and switching loss, shown in (2.9) and (2.10), where the subscript *cd* stands for the conduction loss, and *sw* indicates the switching loss. The detailed equations for calculating $P_{IGBT\_cd}, P_{IGBT\_sw}, P_{diode\_cd}$ and P_{diode_sw} are provided below.

$$P_{loss\_IGBT} = P_{IGBT\_cd} + P_{IGBT\_sw} \tag{2.9}$$

$$P_{loss\_diode} = P_{diode\_cd} + P_{diode\_sw} \tag{2.10}$$

There are two converters in this WT system, namely the generator-side inverter and the grid-side inverter. Based on the converter topology shown in Fig.3, the number of diode/IGBT can be determined. All components are connected in series from a reliability point of view. Thus, the total power loss on these two converters $P_{WT\_conv\_loss}$ can be estimated by the power loss of all diodes and IGBTs:

$$P_{WT\_conv\_loss} = \sum_{n=1}^{n_D} P_{loss\_IGBT} + \sum_{n=1}^{n_G} P_{loss\_diode} \tag{2.11}$$

where n_D and n_G represent the total number of diode and IGBT, respectively.

Since the thermal behavior is one of the important factors that has an influence on the device failure rate, the calculated $P_{WT\_conv\_loss}$ and hourly based ambient temperature data are applied to estimate the junction temperature and the thermal stress factor of a diode and of an IGBT. The thermal resistance and the temperature cycling factor for each diode and IGBT are also considered.

$$T_{j_{IGBT}} = T_C + R_{sa_{IGBT}} P_{WT_{loss_{conv}}} + R_{jh\_IGBT} P_{WT\_loss\_IGBT} \tag{2.12}$$

$$T_{j_{diode}} = T_C + R_{sa_{diode}} P_{WT_{loss_{conv}}} + R_{jh\_diode} P_{WT\_loss\_diode} \tag{2.13}$$

Equation (2.12) and (2.13) calculate the junction temperature of a diode and an IGBT, where T_C is the ambient temperature, and R_{sa} and R_{jh} are the thermal resistances from heat sink to ambient/from junction to heat sink, respectively. The thermal stress factor π_T for a diode or an IGBT can be derived in (2.14) and (2.15).

$$\pi_{T\_IGBT} = \exp\left[1925\left(\frac{1}{298} - \frac{1}{T_{j_{IGBT}} + 273}\right)\right] \tag{2.14}$$

$$\pi_{T\_diode} = \exp\left[3091\left(\frac{1}{298} - \frac{1}{T_{j_{diode}} + 273}\right)\right] \tag{2.15}$$

The temperature cycling factor π_{TC} for a diode or an IGBT can be expressed by (2.16).

$$\pi_{TCi} = \gamma\left(\frac{12N_s}{t(i)}\right) f(\Delta T_b) \times \exp\left[1414\left(\frac{1}{313} - \frac{1}{T_{b\_max} + 273}\right)\right] \tag{2.16}$$

where γ and $f(\Delta T_b)$ have a specific value/expression for a diode or an IGBT, and their values can be found in 0.

Then, the failure rate model for a semiconductor can be derived, by utilizing all the calculated results from above and the method in 0, where the above-mentioned factors that potentially affect the reliability performance for the component failure rate estimation are considered. Other factors such as radiation, heat and electrical stresses, wear-out effect, and production quality are also included. The failure rate models of a diode or an IGBT are expressed in (2.17):

$$\lambda_{j,t} = \sum_{i}^{N_s} (\lambda_{0Th}\pi_{T\,j,t} + \lambda_{0TC}\pi_{TC\,j,t})\pi_{In}\pi_{Pm}\pi_{Pr} \tag{2.17}$$

where $\lambda_{j,t}$ represents the failure rate of component j at time t, N_s is the number of component states; λ_{0Th} and λ_{0TC} are two base failure rate elements of a component, respectively; $\pi_{T\,j,t}$ and

$\pi_{TC\,j,t}$ are the thermal stress factor and the temperature cycling factor of component j at time t, respectively; π_{ln} is the overstress factor used to represent the overstress contribution, determined by the coefficient sensitivity to overstress and the component application field; π_{Pm} represents the factor of component quality; and π_{Pr} is the factor of reliability control reflecting the aging status in the component's life cycle.

$$R_{WT_{conv}}(t) = e^{-\left(\sum_{j=1}^{N_j} \lambda_{j,t}\right)t} \tag{2.18}$$

Finally, the failure rate of the WT converter can be derived, and the converter reliability can be expressed as in (2.18), where N_j represents the total number of devices.

2.3.2. Reliability Model of PV Converters

As shown in Fig.4, a typical PV system, as considered in this chapter consists of a PV array, a dc-dc boost converter, and a dc-ac inverter.

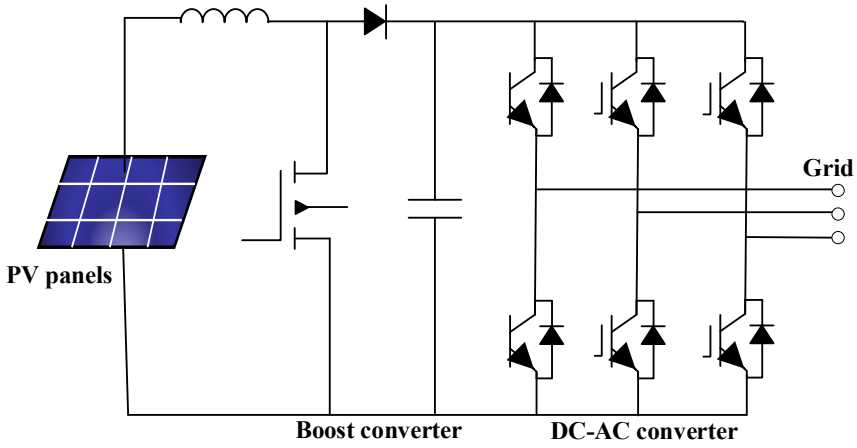

Figure 4. PV system with dc-dc boost converter and dc-ac inverter

Similar to a WT system, the output power of the PV system has a close relationship with the device failure rate. Thus, hourly based input data, such as solar radiance and ambient temperature are collected. Assuming a maximum power point tracking (MPPT) mechanism, the

power produced by PV panels is calculated in equation (2.19), where $P_{pv,t}$ is the power generated by the PV panels at time *t*; S_t is the input solar radiation intensity; S_0 represents the maximum radiation; P_{max} is the maximum power under standard test conditions; γ is the temperature coefficient; T_t is the input ambient temperature, and T_0 represents the standard temperature.

$$P_{pv,t} = \frac{S_t}{S_0} P_{max}[1 + \gamma_0(T_t - T_0)] \tag{2.19}$$

Converters considered in this PV system include a boost, and a dc-ac inverter. Three components, namely a diode, an IGBT and an inductor, are considered in the PV boost converter. The components power losses in the dc-dc boost converter, including conduction loss and switching loss, are calculated similarly compared to WT converter modeling and are presented in (2.20)-(2.22), where $R_{DS(on)}$ is the resistance between the drain and source when the switch is on; f_s is the switching frequency; r_F is the equivalent resistance of the diode; V_F is the forward voltage drop; and r_{es} is the equivalent resistance for the main inductor.

$$P_{pv_{boost_{IGBT}}} = R_{DS(on)} I_{in}^2 + \frac{1}{2} V_{out} I_{in} \left(E_{on} + E_{off}\right) f_s \tag{2.20}$$

$$P_{pv\_boost\_diode} = I_{out}^2 r_F + I_{pv} V_{F0} \tag{2.21}$$

$$P_{pv\_boost\_inductor} = I_{in}^2 r_{es} \tag{2.22}$$

The operating temperature of the main inductor is determined by equations (2.23) - (2.24), where T_{HS} is the hot spot temperature of the inductor, which is a function of its power dissipation and radiating surface area A. T_C represents the case temperature.

$$T_{HS} = T_C + 1.1\Delta T \tag{2.23}$$

$$\Delta \mathrm{T} = 125 P_{pv\_boost\_inductor}/A \tag{2.24}$$

The reliability of PV converter is then presented in (2.25), where N_m represents the total number of devices used in the PV converter, and $\lambda_{m,t}$ is the failure rate of component *m* at time *t*.

$$R_{PV_{conv}}(t) = e^{-(\sum_{j=1}^{N_m} \lambda_{m,t})t} \tag{2.25}$$

2.4. System Level Non-sequential Sampling and Overview

In the proposed power system network, the system-level reliability modeling is realized through a non-sequential Monte Carlo sampling method, which requires less computational time and memory compared with a sequential sampling method [28]-[29].

For each hour, the entire system state is determined through sampling the probability of all components' states. It is assumed that the WT/PV generators have multi states depending on their power output level, and other component has two states: up and down, and that the components are independent from each other. It is worth noting that the components are assumed to be independent because our main focus is to investigate the reliability effect from a power converter perspective. Partially dependent scenarios, such as a cascading failure, are not considered in this chapter.

Since the failure rate is calculated through hourly based data, each component *i* has a failure rate $\lambda_{i,t}$ at hour *t*. The repair rate μ_i is relatively stable and considered as a constant. Each component's up and down state probability can be calculated using (2.26) and (2.27).

$$P_U(i,t) = \frac{\mu_i}{\lambda_{i,t} + \mu_i} \tag{2.26}$$

$$P_D(i,t) = \frac{\lambda_{i,t}}{\lambda_{i,t} + \mu_i} \tag{2.27}$$

Thus, when conducting a non-sequential sampling each hour, each component state can be sampled independently, and the entire system state is determined by the combination of all components' states. Then, DC load flow based linear programming is adopted each hour to calculate the power flows, with the advantages of easy implementation and relatively low

computational cost. Repeat the sampling procedure for a number of simulations until the stopping rule is satisfied. Finally, the estimated system reliability indicators, such as EENS and LOLE are calculated for system analysis.

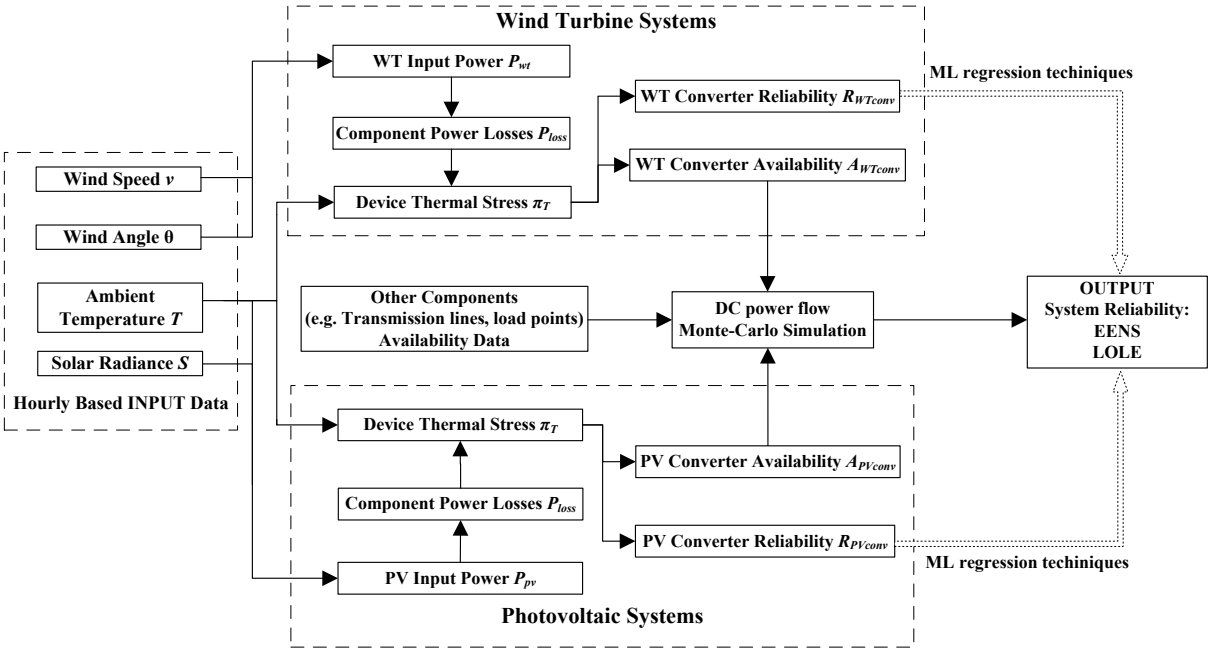

Figure 5. The flowchart of the proposed power system reliability assessment

In Fig. 5, an overview of the proposed framework is presented. First, we collect the hourly-based input data including wind speed, wind angle, solar radiance, and ambient temperature, to estimate the generation power of the WT/PV system throughout one year. Since the power converter consists of various devices, each component's power loss and thermal stress are calculated to derive the time-variant failure rate for each component. Afterwards, the number of each component used in a WT/PV converter is determined based on the converter topology such that all components failure rates are accumulated, and the converter reliability can be predicted. Then, we also consider other reliability data to estimate all component states in the power system.

As shown in Fig. 5, other system components include, but are not limited to, diesel generators, transformers, transmission lines, and load demand. The failure rates of other system

components are assumed to be constant. Thus, after estimating the hourly failure rates of all power converters, all components availability/unavailability can be calculated through the equation (2.26) and (2.27). After determining all component states, we conduct the DC power flow to check the balance of power supply and demand. DC power flow method is a widely used tool for power system analysis which substantially save the computational cost. If part of the load demand is not satisfied, the energy loss will be converted and added onto the system reliability indicators (EENS, LOLE). The reliability mapping between the device and system level is realized through ML regression techniques, which are introduced in the next section with details.

The proposed PDP-based optimization problem for a single EV can be extended to multiple EVs. Besides, the emerging Uber-like EVs will introduce a great amount of temporal-spatial uncertainties to power systems. There is an urgent need to develop sophisticated demand in response to more frequent charging requests.

2.5. Reliability Mapping Through ML Regression Techniques

The development of data science has introduced more applications of artificial intelligence (AI), and ML techniques in diverse fields in recent years [30]. In this chapter, ML regression techniques are implemented for converter level and system level reliability due to the following reasons.

First, to examine the potential effect on system reliability from a power converter perspective, the relationship between power converters and the overall system reliability data are worth investigating; however, due to the high system complexity, this kind of relationship is usually nonlinear such that it is difficult to derive an analytical expression. The ML method is capable of dealing with the nonlinear data relationship, though, because one of the impressive ML capabilities is to approximate the input/output data relationship with arbitrary precision [31].

Second, the relationship may vary as more converters are considered in the power system reliability analysis. ML provides the flexibility for additional parameters to be embedded as another input feature such that the nonlinear relationship can be generalized [32]. Third, system reliability indicators such as EENS and LOLE are considered as the system output labels and they are all continuous. In this work, regression models are preferable compared to classification techniques where the output variable is usually discrete. In this section, basic fundamentals of ML regression and the proposed reliability mapping model are presented.

2.5.1. Theory

From a statistic perspective, the relationship mapping between device and system level reliability data can be modeled as a regression problem. The system reliability indicators are usually treated as system outputs and the reliability of each power converter is considered as one of the input features. The regression logic is described as follows.

Assume that there are *n* pairs of training data in a set $\{(x_k, y_k), k = 1, 2, \dots, n\}$, where x_k is the input feature vector. x_k usually contains an array of data where all data are surrounding a target sample point [28]. The value of this target sample point is calculated from x_k during the testing procedure and is compared with y_k (y_k is continuous), the true value of this sample point. Thus, accuracy is achieved through this comparison. The mapping between input features and output labels is used to investigate an appropriate function from *x* to *y* such that when x_k is known, the value of y_k can be predicted. In the proposed RTS network, all converters reliability data are considered as the input features which are injected into a regression model, and the system reliability indicators are the output labels. The selected ML regression methods are support vector regression (SVR) and random forests (RF). It is worth noting that there are other ML algorithms,

and they may have comparative performance. The purpose of this research is not to find the optimal regression model, but to provide a potential reliability mapping from the device level to the system level through ML techniques.

Algorithm 1 Reliability Mapping Through ML Regression Techniques

Input: Calculated power converter reliability data x, system reliability indices y.

Output: Predicted system reliability indices

Training:

1 A data set is created where vector x denotes all power converter reliability at hour t and y stands for the system reliability index (i.e., EENS, LOLE).

2 Create two ML regression models:

3 $\hat{f}_{SVR} = SVR\ ()$

4 $\hat{f}_{RF} = RandomForestRegression\ ()$

5 Input all the *x* and *y* pairs to each model for training. The ratio of training to testing data is 8:2.

Testing:

6 The trained models are applied to the remaining *x* data and derive the prediction of $\hat{y}$.

7 Use typical indices, such as RMSE and R-squared, to evaluate the mapping models

The main steps of the proposed regression mapping are provided in Algorithm 1. The root-mean-square error (RMSE) and R-squared are used to evaluate the performance of both regression models. RMSE is a standard measure of error when a model predicts quantitative data [32]. The lower RMSE value is, the better prediction is indicated in this regression model. On the other hand, R-squared is a statistical measure that indicates how much a variation of a dependent variable is explained and it ranges from 0 to 1.

In general, if the R-squared value reaches 1, it represents that the implemented regression model is well fitted to the input/output data set. On the contrary, when the R-squared reaches 0, it indicates that the regression model does not fit the data at all.

2.5.2. Support Vector Regression

SVR has mainly been developed for handling nonlinear regression problems. This algorithm is adapted from the ML classification paradigm, namely the support vector machine (SVM) which is operated by maximizing the margin of the decision boundary [33]. In SVR, the first step is to map the input features $x = \{x_1, x_2, \dots, x_n\}$ (with n power converters considered, for example) into an n-dimensional kernel-induced feature space through a fixed mapping method where they are linearly correlated with the output labels. Thus, the SVR model can be described by the following notation:

$$f(x) = \sum_{k=1}^{n} \hat{y}_k g_k(x) + b \tag{2.28}$$

where $\hat{y}_k$ is the predicted system reliability value, $g_k(x)$ denotes the nonlinear transformation, and b stands for the predicted bias value. A cost function is required for the SVR formulation. A robust ε-insensitive loss function is adopted. Detailed mathematical information can be found in [33].

2.5.3. Random Forests

RF is an ensemble learning method developed for improving classification and regression trees through combining a large set of decision trees [34]. Each individual tree is built based on a random subset of the input variables and the predicted output value depends on the average prediction of all aggregated trees. Specifically, an input vector $x = \{x_1, x_2, \dots, x_n\}$ is given to build

the forest. A set of m trees $\{T_1(x), T_2(x), \dots, T_m(x)\}$ is created and all trees predict the output $\{\hat{y}_1 = T_1(x), \dots, \hat{y}_m = T_m(x)\}$. To derive the final result, all trees' predictions are aggregated, and the average value is calculated as in (29). The growing procedure of each tree can be found in [35].

$$\hat{f}(x) = \frac{1}{m}\sum_{k=1}^{m} \hat{y}_k(x) \tag{2.29}$$

2.6. Numerical Analysis

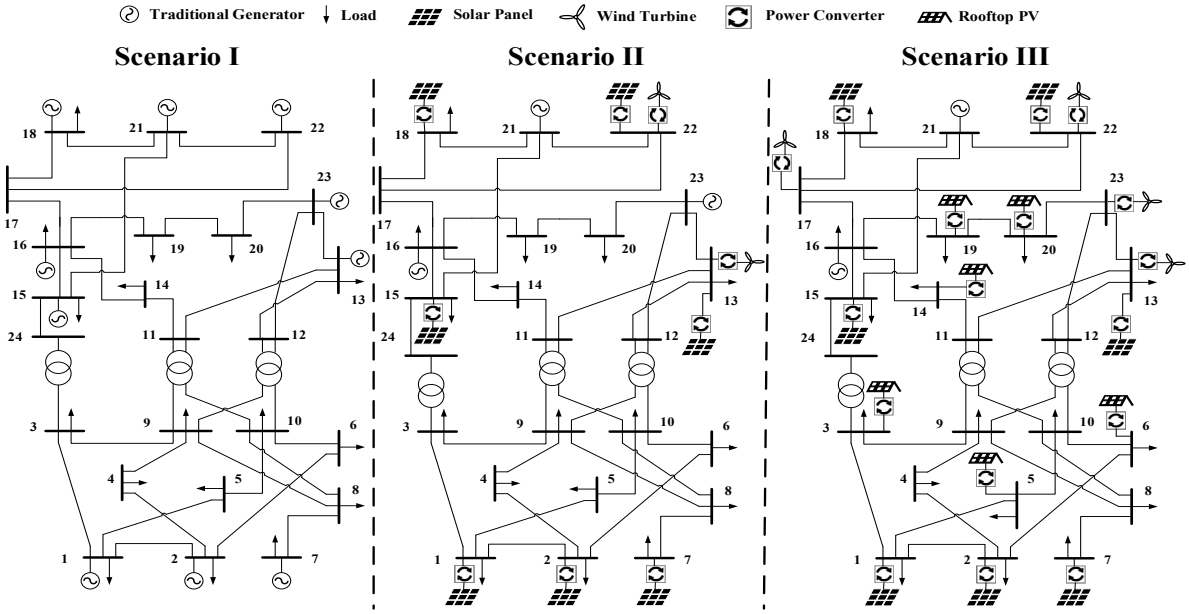

Figure 6. The illustration of RES/power converter penetration in the RTS network

Generators are all conventional in scenario I. Several RESs and connected power converters are implemented in scenario II. More RESs, including rooftop PVs, and power converters are considered in scenario III.

The proposed framework was validated on a system with the following configuration: Intel(R) Core(TM) 16 GB 2.30GHz. The non-sequential MC simulation was performed in Matlab 2019b, and ML regression models were implemented through Python scikit-learn. The collected hourly based data, such as wind speed, solar radiance, and ambient temperature, are provided in [36].

2.6.1. System Description

In numerical analysis, a modified IEEE RTS-24 bus network as shown in Fig.6, is used as the test system. To investigate the penetration of RESs and power electronic converters, three scenarios are considered to reflect converter penetration in a power system:

1) Scenario I: In this scenario, the original RTS is applied as shown on the left side of Fig. 6, where all generators are conventional (e.g., diesel, thermal). Thus, traditional generators dominate the power system generation in this case, and the system reliability is evaluated without considering the RESs and power converters. Other components such as transmission lines and load points are equipped with constant failure rates. The detailed reliability data and load model are provided in [36].
2) Scenario II: This scenario mimics the proliferation of RESs in an RTS network that renewable technology has been developing rapidly in recent years. Specifically, two WT and seven PV systems are implemented to replace conventional generators on different buses, as shown in the middle of Fig. 6. The WT and PV converter reliability models were presented in Section 2.3 with a small rated capacity, such as 2 MW and 0.5 MW, respectively. Thus, the reliability model of each power converter implemented in this scenario can be obtained by combining the reliability of each individual WT/PV converter. For instance, the reliability of a 25.9MW PV on bus 1 can be obtained by combining 52 small converter reliability models where each has a capacity of 0.5MW.
3) Scenario III: This scenario assumes that renewable technologies are sufficiently developed for industrial/residential use in the future, as presented on the right side of Fig. 6. Two more WT systems are considered on buses 17 and 23, respectively. Furthermore, six rooftop PV systems with smaller capacities (around 9 to 12 MW) are

implemented, which results in the total number of power converters considered in this scenario reaching 17. Similar to the previous scenario, a converter reliability with a large capacity can be derived from several converter reliability models where each has a small capacity.

2.6.2. Importance of Considering Converter Reliability

To highlight the importance of considering power converters when evaluating system reliability, traditional system indicators are calculated for all three scenarios, including EENS, and LOLE.

Table 1: Reliability indicator under all scenarios

Scenario	EENS (MWh/yr)	LOLE (days)	Number of Converters
I	695.74	1.94	\
II	4070.38	10.85	9
III	18025.91	22.68	17

Fig. 7 illustrates the accumulated EENS and LOLE for all three scenarios, respectively. The annual values of EENS and LOLE are also summarized in Table 1. In Fig. 7, the EENS and LOLE increase quickly in the last two scenarios while they are maintained at relatively low values in scenario I. This is because of the uncertainty of WT and PV systems, and the power converter failures being introduced in the last two scenarios. Additionally, the EENS in scenario I finally reaches 695.74 MWh/year and LOLE reaches 1.94 days, which are 17.1% and 17.9%, respectively, compared with scenario II, and 3.9% and 8.6% compared with scenario III.

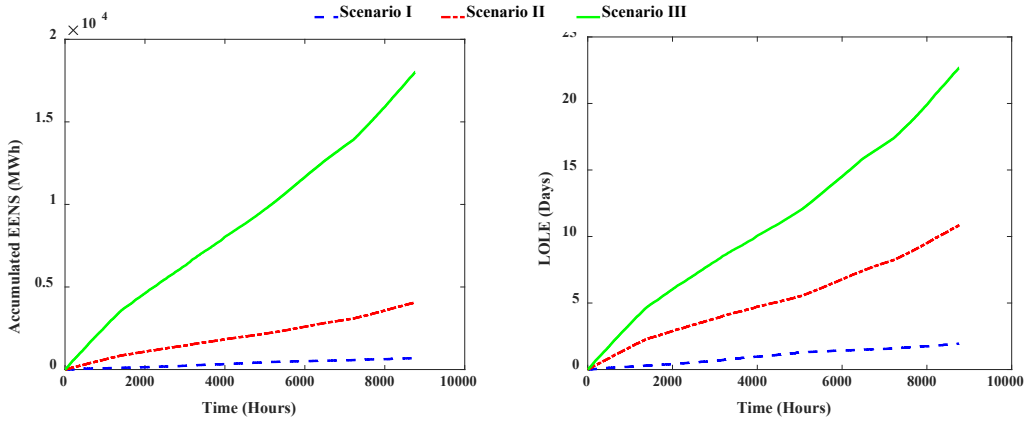

Figure 7. Accumulated EENS of all three scenarios

This shows that the power converter has a non-negligible effect on system reliability. As the number of power converters considered in the power system increases, both EENS and LOLE reach a relatively high value which indicates the system becoming unreliable.

2.6.3. The Reliability Effect of Converter Topologies

The converter topology not only determines how many power electronic devices are used but also reveals how they are connected with each other. Consequently, converter reliability performance can be greatly affected by the choice of converter topology. Thus, only scenario II and III are considered. Three typical converter topologies for high-power WTs and PVs are selected: a three-level cascaded H-bridge (CHB), a neutral point clamped (NPC), and a flying capacitor converter (FCC) [37]-[38]. The total number of various devices used in these topologies are summarized in Table 2. NPC is also known as diode-clamped and more diodes are applied in this topology compared with in the other two topologies. The three-level FCC needs a minimum of four independent capacitors, i.e., a total of two auxiliary capacitors per phase leg in addition to two main dc bus capacitors [37]. The detailed topology information of all three converter topologies can be reviewed in [38].

Fig. 8 illustrates the system EENS while three topologies are applied in scenario II and III, respectively, where the blue dotted line represents CHB, the red dash-dot line is NPC, and the green solid line depicts the FCC topology. The EENS value among all three topologies grow steadily and finally reaches 4070.38 MWh (CHB), 4164.07 MWh (NPC), and 4315.58 MWh (FCC) in Fig.8, which indicates that the converter topologies do have an influence on system reliability, though, this influence is not very critical. Notably, in scenario III, the system EENS with FCC topology grows rapidly during 3000 to 5000 hours (summertime) and then slows down, which indicates an outage is more likely to happen during the summer and more maintenance may be required.

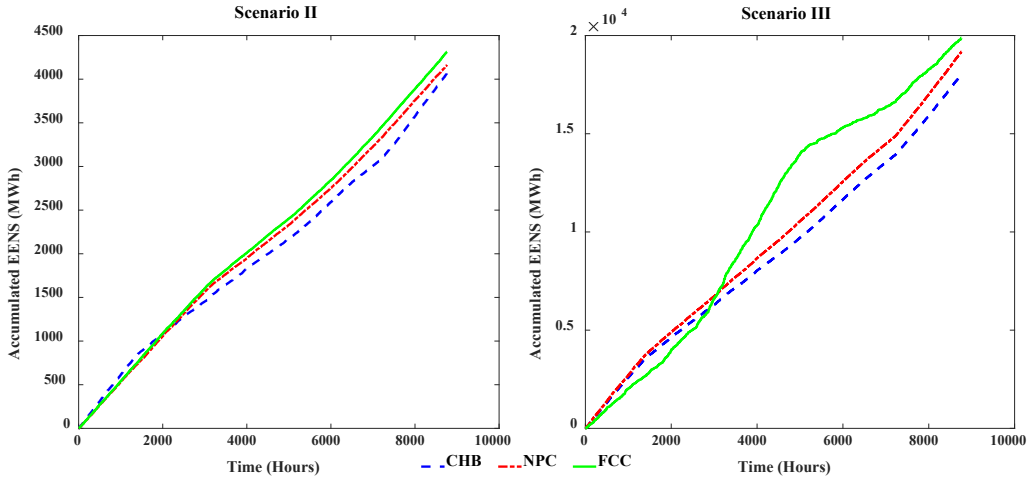

Figure 8. Scenario II EENS under three converter topologies

Table 2: Total number of devices used in different converter topologies

Topology	IGBTs	Diodes	Capacitors
CHB	12	12	3
NPC	12	18	2
FCC	12	12	9

There are other power converter topologies that can be connected with RESs and implemented in a power system. It is to be noted, however, that the purpose of this case is not to

find the optimal converter topology for power converters/system reliability performance, but to investigate system reliability when different converter topologies are applied.

2.6.4. The Regression Mapping between Two Levels

To investigate the hidden relationship between device level and system level reliability, SVR and RF regression models are implemented. In general, 80% of the device/system reliability data is used for training as input variables to the model for intrinsic parameters selection. The remaining 20% is used for testing. The computational time of SVR and RF are 42.78s and 45.64s, respectively. Two statistical measurements: Root Mean Square Error (RMSE), and R-squared, are used to evaluate the effectiveness of the implemented regression methods.

Table 3: ML regression results of SVR and RF

Model	Scenario	RMSE	R-squared
SVR	II	1.943	0.947
	III	2.719	0.892
RF	II	2.221	0.921
	III	2.895	0.883

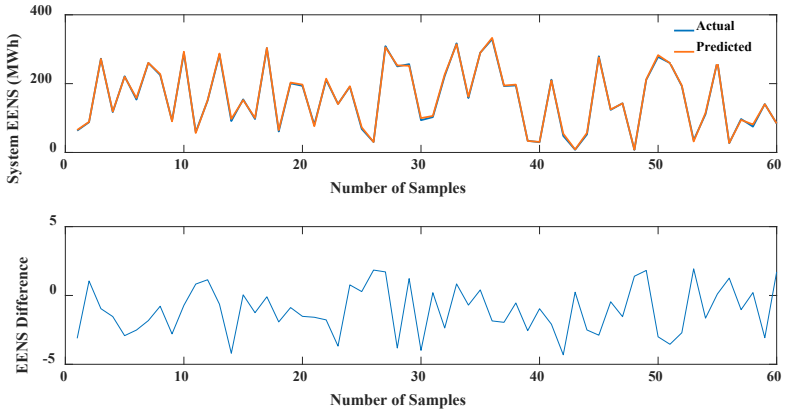

Figure 9. Comparison of the predicted and the actual EENS

In the numerical analysis, the RMSE values under scenario II are all lower than those values in scenario III. This is due to the system complexity, i.e., fewer number of power converters is considered in scenario II. On the other hand, both R-squared values of SVR and RF methods reach above 0.9 in scenario II and 0.88 in scenario III, respectively. As shown in Fig.9, 60 samples of testing data are collected to compare the predicted EENS and the corresponding actual value. The difference between the predicted and actual value is also shown in the same figure.

In general, the predicted EENS follows the actual EENS pattern across all samples, and the maximum difference only reaches 4.31(absolute value). This indicates that it is possible to implement a reliability mapping between the power converter and system level through ML techniques.

2.7. Conclusions

We propose a two-level reliability framework to bridge the gap between power converters and power systems. The reliability performance of a power system is evaluated considering the impact of power converters' reliability. The reliability model of each converter is built from the device level, where critical semi-conductor devices are included. Each converter reliability is used as one of the input features and the system reliability indicators are defined to be the outputs. Furthermore, to investigate the relationship between converter and system reliability, ML regression techniques are used as it is a useful tool to determine nonlinear relationships. The numerical results show that the converter reliability has a non-negligible effect on the modern power system performance, and a nonlinear relationship between multiple power converters and overall system reliability can be built using regression techniques. Future works will focus on investigating the applications of parallel computing to speed up the proposed reliability analysis.

The reliability impact of power converters' internal connections in a RES is also worth investigating. The influence on the power system network changes (i.e., different network topologies) will change the power flow and ultimately affect the system reliability performance. Once the real-world or synthetic transmission networks become available for reliability analysis, one will be able to investigate the scalability of the proposed reliability assessment framework. Moreover, since ML encapsulates the relationship and acts like a 'black box', the integration of ML interpreting methods will be investigated to improve the reliability explanation and provide useful information for system operators. Appropriate reliability requirements on the converter level, and corresponding system maintenance strategies could be investigated.

2.8. References

[1] Yingkui, G. and Jing, L., 2012. Multi-state system reliability: A new and systematic review. Procedia Engineering, 29, pp.531-536.

[2] Zhou, P., Jin, R.Y. and Fan, L.W., 2016. Reliability and economic evaluation of power system with renewables: A review. Renewable and Sustainable Energy Reviews, 58, pp.537-547.

[3] Jaise, J., Kumar, N.A., Shanmugam, N.S., Sankaranarayanasamy, K. and Ramesh, T., 2013. Power system: a reliability assessment using FTA. International Journal of System Assurance Engineering and Management, 4(1), pp.78-85.

[4] Fang, J., Su, C., Chen, Z., Sun, H. and Lund, P., 2016. Power system structural vulnerability assessment based on an improved maximum flow approach. IEEE Trans on Smart Grid, 9(2), pp.777-785.

[5] Arabali, A., Ghofrani, M., Etezadi-Amoli, M. and Fadali, M.S., 2013. Stochastic performance assessment and sizing for a hybrid power system of solar/wind/energy storage. IEEE Trans on Sustainable Energy, 5(2), pp.363-371.

[6] Polo, F.A.O., Bermejo, J.F., Fernández, J.F.G. and Márquez, A.C., 2015. Failure mode prediction and energy forecasting of PV plants to assist dynamic maintenance tasks by ANN based models. Renewable energy, 81, pp.227-238.

[7] Awadallah, S.K., Milanović, J.V. and Jarman, P.N., 2014. The influence of modeling transformer age related failures on system reliability. IEEE Trans on Power Systems, 30(2), pp.970-979.

[8] Ding, Y., Singh, C., Goel, L., Østergaard, J. and Wang, P., 2014. Short-term and medium-term reliability evaluation for power systems with high penetration of wind power. IEEE Trans on Sustainable Energy, 5(3), pp.896-906.

[9] Ahadi, A., Ghadimi, N. and Mirabbasi, D., 2014. Reliability assessment for components of large scale photovoltaic systems. Journal of Power Sources, 264, pp.211-219.

[10] Falahati, B., Fu, Y. and Mousavi, M.J., 2013. Reliability modeling and evaluation of power systems with smart monitoring. IEEE Trans on smart grid, 4(2), pp.1087-1095.

[11] Wang, S., Li, Z., Wu, L., Shahidehpour, M. and Li, Z., 2013. New metrics for assessing the reliability and economics of microgrids in distribution system. IEEE Trans on power systems, 28(3), pp.2852-2861.

[12] Wang, B., Cai, J., Du, X. and Zhou, L., 2017. Review of power semiconductor device reliability for power converters. CPSS Trans on Power Electronics and Applications, 2(2), pp.101-117.

[13] Zhou, D., Wang, H. and Blaabjerg, F., 2017. Mission profile based system-level reliability analysis of DC/DC converters for a backup power application. IEEE Trans on Power Electronics, 33(9), pp.8030-8039.

[14] Sakly, J., Abdelghani, A.B.B., Slama–Belkhodja, I. and Sammoud, H., 2017. Reconfigurable DC/DC converter for efficiency and reliability optimization. IEEE Journal of Emerging and Selected Topics in Power Electronics, 5(3), pp.1216-1224.

[15] Sadeghfam, A., Tohidi, S. and Abapour, M., 2017. Reliability comparison of different power electronic converters for grid-connected PMSG wind turbines. International Trans on Electrical Energy Systems, 27(9), p.e2359.

[16] Jamshidpour, E., Poure, P. and Saadate, S., 2015. Photovoltaic systems reliability improvement by real-time FPGA-based switch failure diagnosis and fault-tolerant DC–DC converter. IEEE Trans on Industrial Electronics, 62(11), pp.7247-7255.

[17] Gupta, N., Garg, R. and Kumar, P., 2017. Sensitivity and reliability models of a PV system connected to grid. Renewable and Sustainable Energy Reviews, 69, pp.188-196.

[18] Ni, K., Hu, Y., Lagos, D.T., Chen, G., Wang, Z. and Li, X., 2019. Highly Reliable Back-to-Back Power Converter Without Redundant Bridge Arm for Doubly Fed Induction Generator-Based Wind Turbine. IEEE Trans on Industry Applications, 55(3), pp.3024-3036.

[19] Fischer, K., Pelka, K., Bartschat, A., Tegtmeier, B., Coronado, D., Broer, C. and Wenske, J., 2018. Reliability of power converters in wind turbines: Exploratory analysis of failure and operating data from a worldwide turbine fleet. IEEE Trans on Power Electronics, 34(7), pp.6332-6344.

[20] Mangu, B. and Fernandes, B.G., 2014, September. Multi-input transformer coupled DC-DC converter for PV-wind based stand-alone single-phase power generating system. In 2014 IEEE Energy Conversion Congress and Exposition (ECCE) (pp. 5288-5295). IEEE.

[21] Tu, P., Yang, S. and Wang, P., 2018. Reliability-and cost-based redundancy design for modular multilevel converter. IEEE Trans on Industrial Electronics, 66(3), pp.2333-2342.

[22] De León-Aldaco, S.E., Calleja, H. and Alquicira, J.A., 2014. Reliability and mission profiles of photovoltaic systems: A FIDES approach. IEEE Trans on Power Electronics, 30(5), pp.2578-2586.

[23] Ceperic, E., Ceperic, V. and Baric, A., 2013. A strategy for short-term load forecasting by support vector regression machines. IEEE Trans on Power Systems, 28(4), pp.4356-4364.

[24] Peyghami, S., Blaabjerg, F. and Palensky, P., 2020. Incorporating Power Electronic Converters Reliability into Modern Power System Reliability Analysis. IEEE Journal of Emerging and Selected Topics in Power Electronics.

[25] Shahidirad, N., Niroomand, M., Hooshmand, R.A., 2018. Investigation of PV power plant structures based on Monte Carlo reliability and economic analysis. IEEE Journal of Photovoltaics, 8(3), pp.825-833.

[26] Nguyen, N., Almasabi, S., Mitra, J. and Shenoy, B.B., 2018, June. Correlation of wind speed and wind turbine reliability in system adequacy assessment. In 2018 IEEE International Conference on Probabilistic Methods Applied to Power Systems (PMAPS) (pp. 1-6). IEEE.

[27] Billinton, R. and Bai, G., 2004. Generating capacity adequacy associated with wind energy. IEEE Trans on energy conversion, 19(3), pp.641-646.

[28] Lei, H. and Singh, C., 2016. Non-sequential Monte Carlo simulation for cyber-induced dependent failures in composite power system reliability evaluation. IEEE Trans on Power Systems, 32(2), pp.1064-1072.

[29] Urgun, D. and Singh, C., 2018. A Hybrid Monte Carlo Simulation and Multi Label Classification Method for Composite System Reliability Evaluation. IEEE Trans on Power Systems, 34(2), pp.908-917.

[30] Duchesne, L., Karangelos, E. and Wehenkel, L., 2017, June. Machine learning of real-time power systems reliability management response. In 2017 IEEE Manchester PowerTech (pp. 1-6). IEEE.

[31] Dragičević, T., Wheeler, P. and Blaabjerg, F., 2018. Artificial intelligence aided automated design for reliability of power electronic systems. IEEE Trans on Power Electronics, 34(8), pp.7161-7171.

[32] Liu, H., Liu, Z., Liu, S., Liu, Y., Bin, J., Shi, F. and Dong, H., 2018. A nonlinear regression application via machine learning techniques for geomagnetic data reconstruction processing. IEEE Trans on Geoscience and Remote Sensing, 57(1), pp.128-140.

[33] Shaker, H., Zareipour, H. and Fotuhi-Firuzabad, M., 2013. Reliability modeling of dynamic thermal rating. IEEE Trans on Power Delivery, 28(3), pp.1600-1609.

[34] Tomin, N., Zhukov, A., Sidorov, D., Kurbatsky, V., Panasetsky, D. and Spiryaev, V., 2015. Random forest based model for preventing large-scale emergencies in power systems. International Journal of Artificial Intelligence, 13(1), pp.211-228.

[35] Benali, L., Notton, G., Fouilloy, A., Voyant, C. and Dizene, R., 2019. Solar radiation forecasting using artificial neural network and random forest methods: Application to normal beam, horizontal diffuse and global components. Renewable energy, 132, pp.871-884.

[36] Grigg, C., Wong, P., Albrecht, P., Allan, R., Bhavaraju, M., Billinton, R., Chen, Q., Fong, C., Haddad, S., Kuruganty, S. and Li, W., 1999. The IEEE reliability test system-1996. A report prepared by the reliability test system task force of the application of probability methods subcommittee. IEEE Trans on power systems, 14(3), pp.1010-1020.

[37] Norambuena, M., Kouro, S., Dieckerhoff, S. and Rodriguez, J., 2017. Reduced multilevel converter: A novel multilevel converter with a reduced number of active switches. IEEE Trans on Industrial Electronics, 65(5), pp.3636-3645.

[38] Watanabe, H., Sakuraba, T., Furukawa, K., Kusaka, K. and Itoh, J.I., 2017. Development of dc to single-phase ac voltage source inverter with active power decoupling based on flying capacitor dc/dc converter. IEEE Trans on Power Electronics, 33(6), pp.4992-5004.

CHAPTER 3

Reliability Ranking and Quantification of Multiple Power Converters

3.1. Introduction

This chapter presents a two-stage methodology to comprehensively assess the reliability performance of a converter-dominated power system. In the first stage, the reliability of each power converter is modeled in an accurate manner. Dynamic behaviors of various integrated semiconductor devices and the converter topology are considered. In the second stage, we calculate system-level reliability indicators through a non-sequential Monte Carlo simulation. Machine learning regression algorithms are integrated between the converter and system level reliability data to establish a nonlinear reliability relationship. Moreover, a variance-based sensitivity analysis is conducted to rank and identify the most influential converter uncertainties with respect to the variance of system reliability indicator. Based on the analyzed conclusions, system operators can take proactive actions to mitigate the potential risk of the system.

The incorporation of renewable energy resources (RES) in power systems has brought several challenges to realizing a reliable power delivery. That said, the proliferation of RES has been significantly accompanied by the penetration of various power electronic converters. Notably, the power electronic converter plays a fundamental role during energy conversion [2]. Consequently, from a reliability point of view, the system has become more complicated compared with a traditional system.

A power system's reliability is defined as a measurement of its ability to cope with customer demands. Reliability assessment of conventional power systems has been widely studied [4]. The reliability of power systems with RESs such as WTs or solar PVs is investigated in [6], [7]. The authors in [8] and [9] conducted a system reliability assessment considering diverse load demands in a large-scale WT system or PV system. However, failures associated with power converters have not raised much attention in most published research works. According to field data and industrial experiences, power converters are one of the frequent sources of failure in many electrical applications [9].

From a power electronics perspective, a power converter reliability is largely determined by the performance of critical components. Many researchers have indeed initiated the reliability evaluation of a power converter from its device composition in the last decade. In [11], the authors conducted efficiency and cost estimations for a typical boost converter under a solar panel system. A reliability assessment for critical devices was performed in [9] considering the topology of a WT converter and its thermal loading. Power converters have been implemented to realize actual power conversions in a power system. However, sufficient power conversion can only increase the amount of power available in a power system. Whether these power inputs can be successfully delivered to the load side and satisfy the demand in future power systems is still questionable.

Based on these surveys from both the power system and power electronics fields, it can be concluded that more uncertainty and complexity are introduced in these power systems compared with traditional methods due to the increasing implementation of converters. A lousy reliability performance on the device/converter level may ultimately result in a system-level failure. In [2] and [13], a fundamental exploration of the reliability impacts on the overall system performance from converter failures is investigated. It is necessary to intensify the importance of power

electronic converters and explore their potential effects when evaluating the system reliability under the proliferation of RESs and power electronic interfaces.

Meanwhile, various uncertain parameters are introduced in power systems due to intermittent RESs and the operational structure. These uncertainties may have a significant influence on the system's reliability performance. The authors in [14] highlighted that a conservative power system assessment or non-optimal maintenance solutions would be made by decision-makers if spatiotemporal uncertainties are neglected. In [15], the authors implemented several numerical sensitivity analysis (SA) methods to investigate the most critical uncertainty affecting the reliability of power systems. Therefore, implementing an appropriate SA on the proposed reliability framework is essential in order to interpret the system reliability behavior and identify the effects that emerging power converters will have on system reliability. Identifying the most critical uncertainties, i.e., the most influential pair of a RES and its connected power converter on the system reliability, will help system operators and stakeholders to better arrange the maintenance schedule and facilitate better system operation.

SA is mainly categorized into two classes: local SA (LSA) and global SA (GSA). GSA has a variety of applications in power systems, such as reconfiguring power networks [16], allocating voltage control devices [18], and improving transmission capacity [19]. However, most conventional GSAs neglect the uncertain parameters from RESs and power converters and may not provide accurate results in terms of system reliability characteristics. In the last decade, a variety of implementations of the variance-based GSA have been presented, which indicates that the variance is a universal and proper index to depict the output variability. Another advantage of variance-based GSA over other GSA method is that system variance has been validated as an

adequate index to quantify the contribution of each input uncertainty without any hypothesis on the linearity or monotonicity of the model 0.

Fig. 10 generalizes each step of the proposed reliability assessment framework. The first stage of the proposed framework utilizes a group of failure rates for various semiconductor devices. After considering various topologies, each power converter's reliability is estimated. In step three, system reliability indicators are calculated through a set of Monte Carlo simulations. Further, in step four, we establish a relationship between the converter and the system stage from the reliability perspective by utilizing machine learning (ML) regression algorithms to capture the converter dependence structure for several devices and calculate the reliability indicators of a converter-dominated power system.

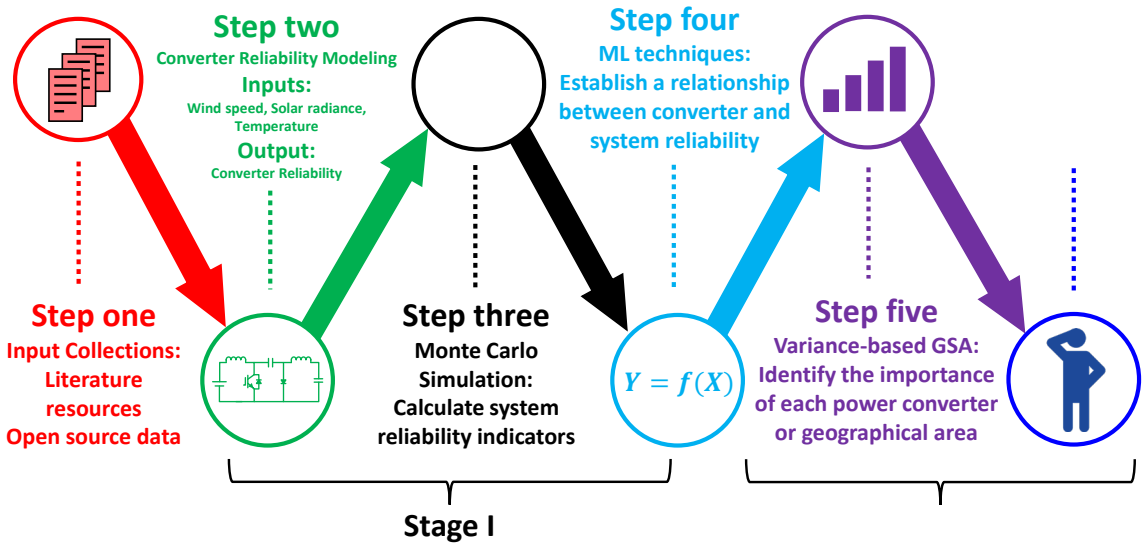

Figure 10. Six steps of the proposed two-stage reliability assessment framework

From the power converter perspective, the second stage of the proposed framework presents for the first time the application of the variance-based GSA to identify the contribution of each converter uncertainty to the variance of the system reliability indicator. This novel application is of critical importance as future power systems become increasingly implemented with RESs and power converters. The research purpose of this stage is to provide instructive information to system

operators, achieve better system operation planning, and promote the application of more advanced SA methods in power systems.

According to the aforementioned reliability and uncertainty issues posed by the proliferation of RESs and power electronic converters in future power systems, this chapter has the following contributions:

1) The reliability performance of each power converter is associated with physical/thermal dynamics of several semiconductor devices and environmental uncertainties. Therefore, the reliability modeling of power converters should be achieved in a more accurate manner. In the first stage of the proposed reliability assessment of a power system, we consider a wide range of semiconductor devices and formulate a reliability model for each device. After considering each power converter topology, we collect the failure rate of each device accordingly, and a comprehensive reliability model of each power converter is derived.
2) Since the increasing integration of power converters in a power system, the impact of converter reliability on the system-level performance is of great importance. This chapter presents a methodology that utilizes ML regression algorithms as a bridge to establish a reliability dependence between the power converter and system-level reliability. The theoretical analyses obtained from this scheme illustrate the significant role of power converters when evaluating system reliability.
3) The uncertainty parameters coming from power converters are yet to be considered when conducting traditional GSA. In the second stage, the variance-based GSA method is applied to the proposed power system to provide instructive information to system operators and stakeholders such that better operational planning can be achieved. This

novel application is also intended to promote the development of the implementation of more advanced SA methods in power systems so that interested researchers can further interpret the system reliability behavior.

In the following, first, the formulation of power converter reliability is summarized in Section 3.2. Concepts about ML and two regression algorithms are introduced in Section 3.3. Section 3.4 introduces the fundamental procedure of how the variance-based GSA is integrated into the power system. Next, we conclude the Monte Carlo simulation and illustrate a system overview. The proposed reliability framework is verified on the IEEE 24-bus RTS in Section 3.5. Conclusions and future works are summarized in Section 3.6.

3.2. Formulation of Converter Reliability

The reliability of every power electronic converter should be quantified in an accurate manner. The reliability value *R(t)* is conventionally estimated by (3.1), where λ is the failure rate, which was time-invariant and usually defined as a constant throughout the year [9].

$$R(t) = e^{-\lambda t} \tag{3.1}$$

However, the failure rate value is mostly affected by various uncertainties, such as ambient variations and component thermal loadings. To consider these factors, we collect hourly based ambient data and assume each uncertainty follows a pre-defined probability distribution over a 1-year time span such that in each converter, the values of λ and *R(t)* are determined in a more accurate manner. General steps of converter reliability modeling are shown in Algorithm 2. An explanation of the formulation procedure is also provided. The detailed converter schematic and calculations can be found in [13].

Both wind power and PV systems are included in the proposed network. Two converters are considered in each WT system: the grid-side and the generator-side inverter. Meanwhile, a DC-DC boost converter and a DC-AC inverter are considered in the PV system.

In each hour, the WT output power P_{WT} depends on the wind speed [6], while the PV output power P_{PV} is determined by the solar radiance and the ambient temperature. Consequently, the power loss of each semiconductor device varies and ultimately affects its failure rate value.

Based on the observation of WT/PV converter topologies, diodes, and IGBTs are mainly considered as critical semiconductors. The number of diodes/IGBTs used in each converter can be determined accordingly.

Algorithm 2: Reliability of WT/PV converters

Input: Hourly based data, including wind speed v, ambient temperature T, and solar radiance SR

Output: WT/PV converter reliability $R_{WT_{conv}}$ / $R_{PV_{conv}}$ and availability $A_{WT_{conv}}/A_{WT_{conv}}$

Steps:

1. An hourly-based data set of v, T, and SR is collected with a one-year time span.
2. Calculate the input power of WT/PV: P_{WT}/P_{PV}
3. Determine the type and number of each semiconductor device considering the topologies of WT/PV converter
4. Estimate the power loss of each device (conduction or switching loss)
5. Calculate other parameters such as thermal stress and device aging factors
6. Determine the failure rate of each semiconductor device
7. Based on the WT/PV converter topologies, calculate $R_{WT_{conv}}/R_{PV_{conv}}$ and $A_{WT_{conv}}/A_{WT_{conv}}$

Afterward, we estimate the total power losses of each device in each converter. The total power losses are determined by the combination of conduction loss P_{cd} and switching loss P_{sw}, and they are calculated through a variety of parameters such as voltage drops, resistance, and the

switching frequency [1]. The detailed equations for calculating $P_{IGBT\_cd}, P_{IGBT\_sw}, P_{diode\_cd}$ and P_{diode_sw} are also provided in [13].

Device thermal behaviors such as stress factor and junction temperature are critical parameters having an impact when calculating a device failure rate. Hence, together with the ambient temperature, the calculated power losses are collected to calculate those factors of either a diode or of an IGBT. Temperature cycling factor and thermal resistance are also considered for each device.

Afterward, the device failure rate model is built through the method mentioned in 0 and all the calculated results from above and where various factors which potentially affect the reliability performance are considered. The failure rate model of a semiconductor device can be estimated by (3.2):

$$\lambda_{device} = \sum_{i}^{N_s} (\lambda_{0Th}\pi_{Thi} + \lambda_{0TC}\pi_{TCi})\pi_{In}\pi_{Pm}\pi_{Pr} \tag{3.2}$$

where N_s denotes the number of component states; both λ_{0Th} and λ_{0TC} are base failure rate of a component under the design condition, respectively; π_{Thi} and π_{TCi} are temperature-dependent coefficients under state i, namely thermal stress factor and temperature cycling factor, respectively; The overstress factor π_{ln} is applied to represent the contribution of overstress; π_{Pm} denotes the device quality and its value is assumed to be between 1.6 and 1.7; A normal device life age is assumed and π_{Pr} is used to reflect the device's aging effect.

The WT/PV converter failure rate can be derived after applying (3.2) to each semiconductor device, and then the reliability of each converter can be estimated. It is worth noting that various uncertainties are considered during the converter formulation, not only for a comprehensive converter reliability estimation but are further utilized to help conduct the system

SA in the numerical analyses, where the most influential converter to the system reliability performance is identified.

3.3. Applying ML Algorithms for Reliability Mapping

In the proposed framework, we integrate ML regression algorithms between the power electronic converter and power system stage for a reliability mapping due to the following reasons.

Firstly, the potential reliability effect on the system scale from a power converter perspective is worth investigating. However, the complexity of a system reliability assessment/evaluation increases if more power converters are implemented in this system. This type of relationship is assumed to be nonlinear, and hence, it is tough to analytically achieve a general expression or quantify the reliability effect. However, ML techniques are capable of handling this type of relationship. An impressive feature of ML techniques is their capabilities of establishing a relationship between multiple input features and output labels with arbitrary precision 0. Secondly, this relationship may need an update if new converters will be implemented in the power system in the future. ML can guarantee flexibility when additional input features are embedded. Consequently, we can generalize this nonlinear relationship without too much additional computational cost. Thirdly, we calculate the system LOLE and EENS as the system reliability indicators. They are also performed as ML output labels, and both of them are continuous parameters. Thus, regression algorithms are more appropriate instead of classifications, where the output category is usually discrete. The following three subsections introduce the fundamental logic of ML and two regression algorithms applied in the proposed framework.

In ML techniques, the mapping refers to investigate an appropriate function from X to Y where X represents the set of input features and Y is the set of output labels, such that the value of Y_k can be predicted when X_k is given. In this research, each power converter's reliability data is

collected as one of the input features, while system EENS or LOLE are assumed as the output labels.

In the following, the logic of the regression algorithm is introduced. Assume that a set of $\{(x_k, y_k), k = 1, 2, \dots, n\}$ contains n pairs of data where x_k is the input feature vector and y_k represents the system output vector. x_k consists of a data array where all data is surrounding a sampling target y_k' 0. During each testing iteration, we calculate the value of this sampling target based on x_k. The true value of this sampling point y_k is then applied to compare with the calculated y_k'.

Two ML regression methods are selected as candidates to conduct the reliability mapping: support vector regression (SVR) and random forests (RF). The reason for selecting these two algorithms includes accessible guidelines and well-established tools. There exist other regression techniques that are capable of handling this condition. However, the proposed framework's main target is not to define the most effective regression algorithm but explore the possibility of reliability mapping from the converter to system scale.

As defined in 0, SVR is adapted from the support vector machine, which is an ML classification paradigm, and utilizes a subset of the provided dataset to build a function estimator. For the training data $\{(x_1, y_1), \dots, (x_n, y_n)\}$, the ε-insensitive SVR is capable of finding a loss function where the deviation from the target output is limited within ε at all times. Hence, the SVR model is described in equation (3.3) and (3.4):

$$f(x) = w^T \phi(x) + b \tag{3.3}$$

$$L(\xi) = \begin{cases} 0, & |\xi| \le \varepsilon \\ |\xi| - \varepsilon, & |\xi| > \varepsilon \end{cases} \tag{3.4}$$

where $w \in R^n$ is a weighting vector, $\phi(x)$ indicates the mapping transforming function, and b represents the intercept value. ξ represents the deviation. The detailed formulation can be referred to in 0.

Algorithm 3: Conduct a Reliability Mapping by utilizing SVR & RF

Inputs: Reliability data x of all power converters, calculated system reliability indicators y.

Outputs: Prediction of system reliability indicators

Training:

1 Create a data array $X = \{x_1, x_2, \dots, x_n\}$ where each vector x_n denotes the No.n power converter reliability index at time t.

2 Create a data set *Y* for the system EENS and LOLE.

3 Apply ML regression algorithms:
$\hat{f}_{SVR}$ =*SVR* ()
$\hat{f}_{RF}$ =*RandomForestRegression* ()

4 Train the X and *Y* pairs through SVR and RF. The training and testing ratio are set as 8:2.

Testing:

5 Apply both trained models to the remaining data and calculate the predicted output $\hat{y}$.

6 Calculate RMSE and R-squared values to evaluate the effectiveness of both mappings

RF is defined as an ensemble algorithm that combines the prediction of several decision trees. The principle of RF is called bootstrap aggregation, where bootstrap samples are randomly selected from the training data and fitted to a regression tree. As shown in equation (3.5), after all individual trees in an ensemble are fitted, the final decision is determined by aggregating over the ensemble, i.e., calculating the average of the predicted output $\hat{y}_k$. The detailed generation of each decision tree is listed in 0.

$$\hat{f}(x) = \frac{1}{m}\sum_{k=1}^{m} \hat{y}_k(x) \tag{3.5}$$

$$RMSE = \sqrt{\frac{1}{n}\sum_{k=1}^{n}(y_k - \hat{y}_k)^2} \tag{3.6}$$

$$R_{-squared} = 1 - \frac{\sum_{k=1}^{n}(y_k - \hat{y}_k)^2}{\sum_{k=1}^{n}(y_k - \bar{y}_k)^2} \tag{3.7}$$

The proposed regression mapping procedure is provided in the Algorithm 3. The root-mean-square-error (RMSE) and R-squared 0 are calculated through (3.6) and (3.7), respectively, to evaluate the mapping performance of both regression models.

3.4. Variance-based Global Sensitivity Analysis

Since various uncertain parameters are involved in the nonlinear reliability relationship built in the first stage, an appropriate SA is essential to interpret the system behavior based on the information revealed by this relationship. More uncertainty parameters will be involved due to the proliferation of RESs and power electronic converters. However, it is computationally expensive, and it may not be necessary to monitor all uncertainties. Hence, identifying the most critical uncertainties, i.e., the most influential pair of a RES and its connected power converter on the system reliability, will help system operators and stakeholders to better arrange the maintenance schedule and facilitate better system operation. The variance is a universal and useful index to depict the output variability without any hypothesis on the linearity or monotonicity of the model 0. Therefore, in this stage, we apply the variance-based GSA to the proposed power system.

The variance-based GSA investigates the contribution of each uncertain input to the selected output variance, either a single input variable or multiple-input combinations. This method has been applied to a variety of problems in the power system field, such as generators/loads ranking and distributed generation allocation. However, there are few papers that

take power converter uncertainties into consideration when applying variance-based GSA. It is necessary to conduct an importance ranking from the power converter perspective, to improve the understanding of the power system reliability and further provide useful advice for the system operator.

The theoretical background of the variance-based GSA algorithm is first introduced. The detailed specifications, such as the input uncertainties and sensitivity indices are also defined.

3.4.1. Theoretical Background

From a black-box perspective, any model can be described by equation (3.8), where $\boldsymbol{X} = \{X_1, X_2, \dots, X_n\}$ is a vector of n uncertain inputs, and Y is a selected univariate output.

$$Y = g(X_1, X_2, \dots, X_n) \tag{3.8}$$

$$Var(Y) = \sum_{i=1}^{n} V_i + \sum_{1 \le i < j}^{n} V_{i,j} + \cdots + V_{1,2,\dots,n} \tag{3.9}$$

Each input X_i follows a specific probability density function (PDF) and the variance $Var(Y)$ of Y can be decomposed as in equation (3.9) where V_i is the variance of Y caused by X_i without considering its interaction with other uncertain inputs, and $V_{1,2,\dots,n}$ represents the proportion of $Var(Y)$ caused by $\{X_1, X_2, \dots, X_n\}$.

From a power electronic converter perspective, the operating condition of a power converter can be described from the following parameters [9]: peak current, switching frequency, mean junction temperature, etc. In stage I, we can conclude that the converter voltage/current can be calculated from environmental data such as wind speed v and solar radiance S, and the junction temperature can be obtained from equation (X) given the ambient temperature value. Thus, regarding a WT converter i, the input uncertainties consist of wind speed v and temperature T, i.e.,

$X_i = \{v_i, T_i\}$. The solar irradiance S and temperature T represents the uncertainties in a PV converter j ($X_j = \{SR_j, T_j\}$). The switching frequency of a power converter is assumed stable and not considered as an uncertainty.

The traditional reliability index $EENS$ is used as the system output in the first stage, and its variance can be easily obtained. Thus, the variance of $EENS$ is selected as the output $Var(Y)$ in the second stage.

3.4.2. Sensitivity Indices

As described in equation (3.10), we have the Sobol' indices 0 defined as follows:

$$S_i = \frac{V_i}{Var(Y)}, S_{ij} = \frac{V_{i,j}}{Var(Y)}, S_{1\dots k} = \frac{V_{1,2\dots,k}}{Var(Y)} \tag{3.10}$$

where S_i is the first-order index, $S_{i,j}$ is the second-order index, and $S_{1,2,\dots,k}$ is the higher-order index corresponding to $\{X_1, X_2, \dots, X_k\}$. Interactions of this kind will continue up to nth order for n uncertainties.

Thus, the number of indices and computational cost will increase dramatically if calculating the higher-order index. As a result, the first-order and total-effect Sobol' indices are commonly used.

1) First-order index—S_i: According to equation (3.10), the first-order index describes the contribution to the output variance of the effect from X_i, i.e., the effect of a single converter uncertainty to the system variance of $EENS$. Equation (3.11) is used to calculate each S_i 0:

$$S_i = 1 - \frac{E[V(Y|X_i)]}{Var(Y)}, \quad S_i \in [0,1] \tag{3.11}$$

where $E[V(Y|X_i)]$ denotes the expectation of the conditional variance of Y given X_i has a fixed value. This conditional expected variance is taken over all $X_j, j \neq i$, weighted by the density of X_i.

2) Total effect index—TE_i: As described in equation (3.10), there exist interaction terms such as $V_{i,j}$ and higher-order variance that represent the combined effect of multiple inputs. For a system with independent inputs, the total output variance can be described in (12):

$$\sum_i S_i + \sum_i \sum_{i<j} S_{i,j} + \sum_i \sum_{i<j} \sum_{j<k} S_{ijk} + \cdots = 1 \tag{3.12}$$

where S_i is the first-order index. $S_{i,j}$ is the second-order interaction index related to input i and j. Similarly, $S_{i,j,k}$ is the third-order interaction index.

The total effect index TE_i is defined as the sum of all terms in (3.12) that contain the subscript i, which describes the percentage of variance that remains if all inputs except X_i are specified and only X_i is a random variable. Thus, the total effect index can be calculated by equation (3.13):

$$TE_i = \frac{E[V(Y|X_{-i})]}{Var(Y)} \tag{3.13}$$

in which X_{-i} represents the vector of all X_j where $j \neq i$ (i.e., all parameters except X_i).

3.5. Numerical Analysis

In this section, the proposed two-stage framework is validated on the modified 24-bus IEEE reliability test system (RTS). The computations, including non-sequential Monte Carlo simulations, are conducted in Matlab 2020a on an Intel Core at 2.90GHz with 16 GB RAM. ML

regression algorithms are integrated through Python sckit-learn. A well-established software called SIMLAB 0 is adopted for the GSA calculations.

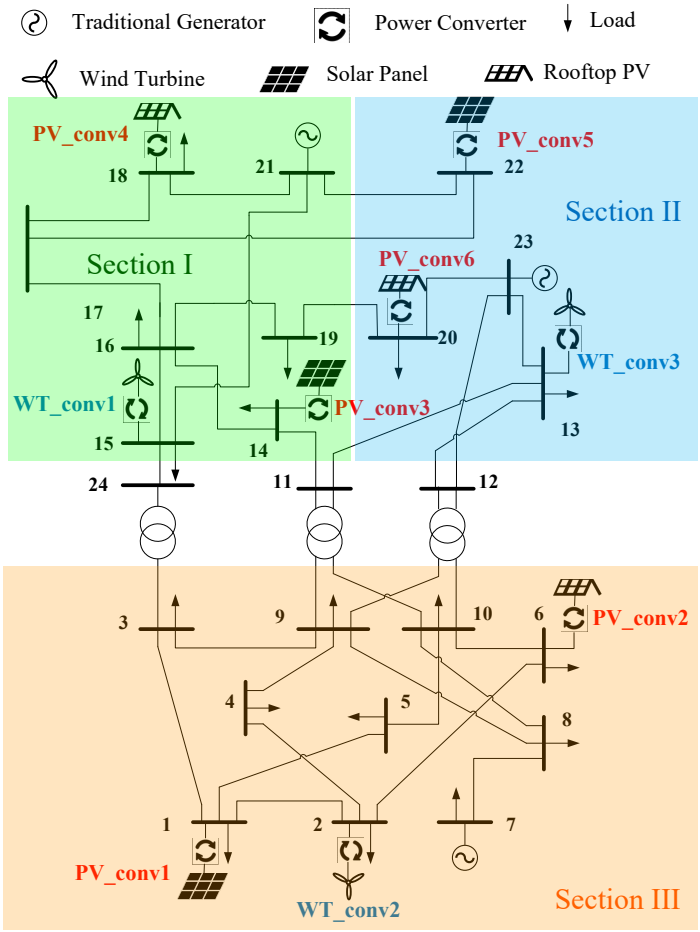

Figure 11. The modified 24-bus IEEE RTS with RES and power converter penetration

3.5.1. The Modified 24-bus IEEE RTS

Fig.11 presents the modified 24-bus IEEE RTS network. The generation and load data are available in 0. Three WT and six PV generators and connected power converters have been added to the system. They are located on different buses with different capacities.

3.5.2. The Reliability Mapping between Two Stages

To conduct the reliability mapping between converter and system scale, SVR and RF algorithms are utilized. As predefined in Algorithm 2, we collect 80% of the converter/system reliability data for the training procedure. The other 20% data set is consequently applied for testing both models. The computational costs are 41.76s and 43.52s for the SVR and RF, respectively. Two statistical measurements, namely RMSE and R-squared, are applied to assess the effectiveness of both implementations.

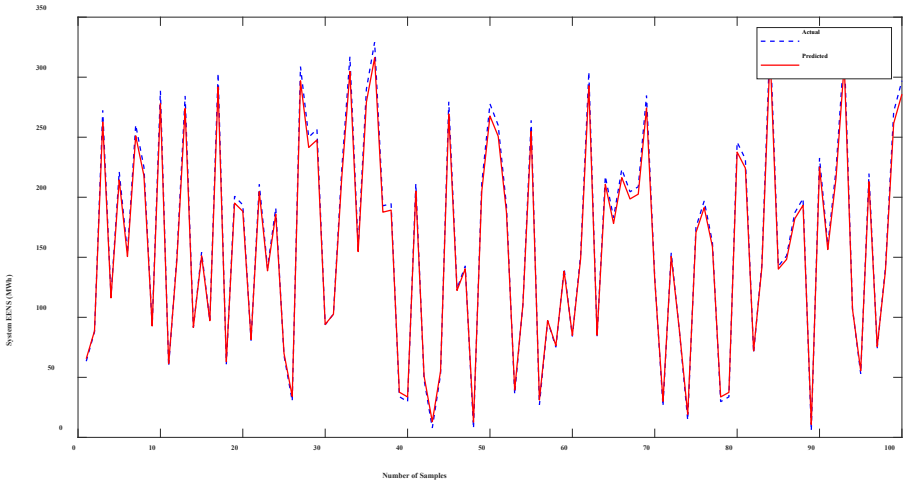

Figure 12. Comparison between the predicted and actual EENS

The RMSE derived from the SVR method is 1.943, which is lower than the value calculated by the RF method (2.221), while the R-squared value under SVR has a higher value, which reaches 0.947 (0.921 under RF). Both R-squared values are above 0.9, which indicates that the predicted and actual system EENS values are basically matched with minimal error. As illustrated in Fig.12, the predicted and the corresponding real EENS are compared in 100 samples of testing data. As a result, the prediction values basically follow the actual pattern under most selected samples. The largest deviation reaches only 1.2%, which indicates that establishing a nonlinear reliability

mapping is possible with the power converter reliability data as inputs and system reliability indicators as outputs through regression algorithms.

3.5.3. Variance-based GSA Results and Maintenance Suggestions

To thoroughly conduct an importance ranking for converter uncertainties on the proposed power network, three cases are considered when implementing variance-based GSA:

Case Study 1. To focus on the analysis of each type of power converter, we consider the uncertainties of all six PVs and their converters which are marked as "PV_conv" in Fig.3.

Case Study 2. We consider new uncertainties from three WT systems ("WT_conv" in Fig.12) such that all converter uncertainties are considered in this case.

Case Study 3. The network is divided into three sections as shown in Fig.11, where each area includes both WT and PV converters. Moreover, we consider the load perturbation on each bus, e.g., between 2% and 5% 0. The uncertainties in each section are grouped together to investigate their importance.

The analyzed results, i.e., the importance ranking under all three cases, can provide system reliability evaluation from the converter perspective so that system operators or stakeholders can identify the most uncertain/vulnerable converter or area and make proactive decisions.

Case study 1: In the first case, utility solar panels and rooftop PV systems are considered. The solar radiance SR and temperature T are used to represent the PV converter uncertainties. Beta and normal distributions are adopted for solar radiance and ambient temperature through $[a, b]$ and $[\mu, \sigma]$, respectively 0.

Table 4 presents the $S1$ and TE values of all six PV converter uncertainties under different numbers of samples. The subscripts with parentheses indicate the rank of each PV converter. Both $S1$ and TE values provide almost identical results that the uncertainties of "PV_conv3" located at bus 14 have the largest values, i.e., 0.128 and 0.481, respectively, which indicates that this converter is of the most importance among all PV converters. From the results of TE, "PV_conv1", "PV_conv3" and "PV_conv5" have higher values, so that these three PV converters are more important compared with the remaining three converters, in terms of the effect on system EENS variation. This is consistent with the fact that rooftop PVs such as "PV_conv6" has a smaller capacity and its failure results in less EENS compared with other utility PVs.

From the system reliability point of view, it can be concluded that the utility PV converters at buses 13, 22, and 1 are more important compared with the remaining three rooftop PV systems.

Table 4: Sensitivity indices of PV converters under different sample sizes

(e.g., $S_{PV_{conv1}} = 0.103_{(3)}$ indicates the first-order index is 0.103 and this PV converter is ranked No.3 among all PV converters)

No. of Samples	First-order indices $[S_{PV_{conv1}}, S_{PV_{conv2}}, \dots, S_{PV_{conv6}}]$	Total-effect indices $[TE_{PV_{conv1}}, TE_{PV_{conv2}}, \dots, TE_{PV_{conv6}}]$
50	$[0.103_{(3)}, 0.079_{(6)}, 0.119_{(1)}, 0.094_{(4)}, 0.113_{(2)}, 0.091_{(5)}]$	$[0.456_{(3)}, 0.313_{(6)}, 0.477_{(1)}, 0.382_{(4)}, 0.468_{(2)}, 0.341_{(5)}]$
100	$[0.102_{(3)}, 0.082_{(6)}, 0.114_{(1)}, 0.092_{(5)}, 0.113_{(2)}, 0.093_{(4)}]$	$[0.452_{(3)}, 0.314_{(6)}, 0.480_{(1)}, 0.391_{(4)}, 0.462_{(2)}, 0.342_{(5)}]$
500	$[0.105_{(3)}, 0.086_{(6)}, 0.124_{(1)}, 0.100_{(4)}, 0.111_{(2)}, 0.093_{(5)}]$	$[0.448_{(3)}, 0.308_{(6)}, 0.478_{(1)}, 0.390_{(4)}, 0.464_{(2)}, 0.340_{(5)}]$
1000	$[0.107_{(3)}, 0.084_{(6)}, 0.127_{(1)}, 0.098_{(4)}, 0.114_{(2)}, 0.095_{(5)}]$	$[0.449_{(3)}, 0.311_{(6)}, 0.481_{(1)}, 0.398_{(4)}, 0.462_{(2)}, 0.341_{(5)}]$
2000	$[0.110_{(3)}, 0.083_{(6)}, 0.128_{(1)}, 0.097_{(4)}, 0.112_{(2)}, 0.094_{(5)}]$	$[0.449_{(3)}, 0.312_{(6)}, 0.480_{(1)}, 0.394_{(4)}, 0.462_{(2)}, 0.343_{(5)}]$

Case study 2: Based on case study 1, we add the uncertainties of all three WT systems in the second case. As described in Section IV, the wind speed v and temperature T are modeled as WT converter uncertainties. Weibull and normal distributions are adopted for wind speed and ambient temperature through $[\alpha, \beta]$ and $[\mu, \sigma]$, respectively 0.

As shown in Fig. 13 and Fig. 14, the sensitivity indices such as first-order $S1$ and total-effect index TE are calculated for all converter uncertainties under 1000 and 2000 sample size. The $S1$ and TE indices provide identical results that WT converter 1 located at bus 15 has the largest $S1$ (0.173) and TE (0.380) values among all the converters, which indicates "WT_conv1" is the most important among all converters. "WT_conv3" located at bus 13 and "PV_conv3" at bus 14 are ranked at 2nd and 3rd place, respectively.

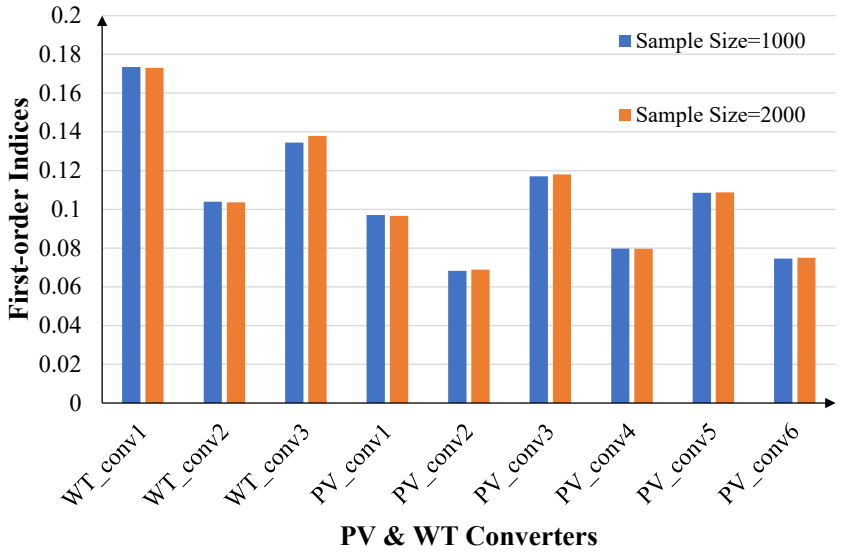

Figure 13. First-order indices of PV/WT converter uncertainties

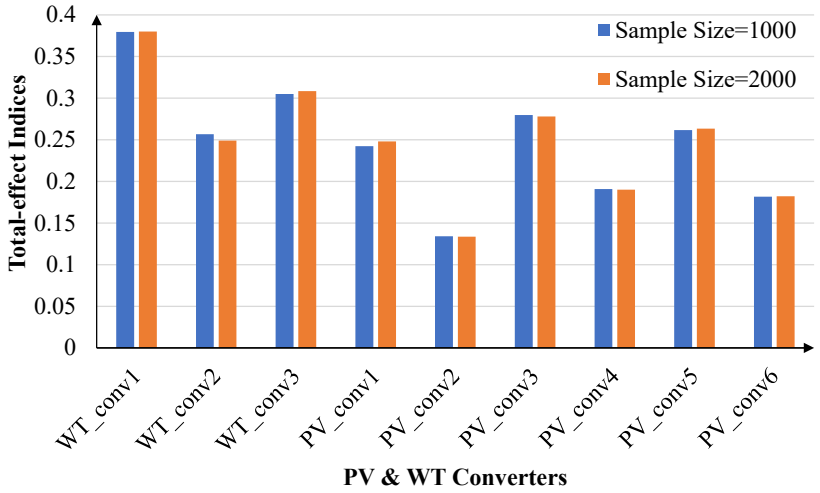

Figure 14. Total-effect indices of PV/WT converter uncertainties

To explain the simulation results from the system network perspective, the "WT_conv1" has the largest capacity, while the "PV_conv2" has the lowest. Further, the WT generation on bus 15 normally will deliver power to several loads on different buses, such as bus 14, 16 and 18, while the "PV_conv2" supplies only a small load on bus 6. Thus, the system EENS does not vary much if a generation fluctuation occurs on "PV_conv2" or a failure happened on this converter.

In conclusion, the converter uncertainty of "WT_conv1" is ranked as the most important affecting the system EENS variance, and the system operator should pay more attention to the WT system located at bus 15.

Case study 3: The system EENS may vary significantly due to a group of uncertainties in a specific geographical area. With increasing converters and loads integrated into the power system, it is desirable to conduct variance-based GSA in different areas, in which multiple converters' uncertainties and load perturbations are considered. In this case, the system network is divided into three sections, I, II, and III, as shown in Fig. 12. Each section contains WT, and PV converters and several loads. Moreover, we introduce a 3% load perturbation on each bus. All uncertainties in each section, hence, are grouped together for consideration in this case. Since the first-order and total-effect indices provided almost identical results in previous cases, only the total-effect index is used in this case to save computational cost. This case is intended to highlight which area should receive more attention and where the maintenance should be primarily scheduled.

Table 5: Bus information of each section

	Involved Buses
Section I	14, 15, 16, 17, 18, 19, 21
Section II	13, 20, 22, 23
Section III	1, 2, 3, 4, 5, 6, 7, 8, 9, 10

Table 5 lists the distribution of all buses in each section, and Table 6 presents the total-effect index under different sampling sizes. Each subscript indicates the section ranking. All TE

values are stable and the TE value on section I is the highest among all three sections under different sample sizes since both "WT_conv1" and "PV_conv3" are located within Section I and are top-ranked based on the results from the previous two cases, which significantly increases the importance of this section. Section III contains more buses compared to the other two sections. However, it has the lowest TE value. The average load demand in I is the highest, while section III has the smallest load requirement. Thus, intuitively, the system EENS variance is more sensitive to section I.

Table 6: Total-effect indices for each divided area

No. of Samples	Sections I	II	III
50	$1.271_{(1)}$	$1.065_{(2)}$	$0.874_{(3)}$
100	$1.276_{(1)}$	$1.041_{(2)}$	$0.865_{(3)}$
500	$1.272_{(1)}$	$1.040_{(2)}$	$0.853_{(3)}$
1000	$1.296_{(1)}$	$1.057_{(2)}$	$0.870_{(3)}$
2000	$1.289_{(1)}$	$1.053_{(2)}$	$0.860_{(3)}$

Since resources are limited, maintenance efforts should be optimally distributed into multiple sections. Thus, the results from this area-based analysis provide a more comprehensive importance ranking, which can help the system operator understand the ultimate effect on system reliability resulting from the uncertainties of a geographical area. This case evaluates the converter uncertainty and load fluctuation of each section and thus, is critical for system operators in scheduling better maintenance and mitigating potential failure risk.

3.6. Conclusions

A two-stage framework is proposed for evaluating the reliability of a power system. In the first stage, we model the reliability of each power converter comprehensively, considering its topology and critical semiconductor devices it is composed of. Afterward, a nonlinear relationship

is established through ML regression techniques. A variance-based GSA is applied in the second stage to conduct an importance ranking for different groups of power converters. The numerical results validate the premise that converter uncertainties have a significant effect on system reliability performance. Future works include but are not limited to focus on investigating reliability's influence on specific converter failures (i.e., aging effects). Moreover, the implementation of ML interpreting algorithms will be explored and provide an explanation of each consequence which results in the system failure.

3.7. References

[1] Peyghami, S., Blaabjerg, F., Palensky, P., 2020. Incorporating power electronic converters reliability into modern power system reliability analysis. IEEE Journal of Emerging and Selected Topics in Power Electronics.

[2] Hou, K., Jia, H., Xu, X., Liu, Z., Jiang, Y., 2015. A continuous time Markov chain based sequential analytical approach for composite power system reliability assessment. IEEE Trans on Power Systems, 31(1), pp.738-748.

[3] Nguyen, N. and Mitra, J., 2017. Reliability of power system with high wind penetration under frequency stability constraint. IEEE Trans on Power Systems, 33(1), pp.985-994.

[4] Zhang, P., Wang, Y., Xiao, W., Li, W., 2012. Reliability evaluation of grid-connected photovoltaic power systems. IEEE Trans on sustainable energy, 3(3), pp.379-389.

[5] Ding, Y., Singh, C., Goel, L., Østergaard, J., Wang, P., 2014. Short-term and medium-term reliability evaluation for power systems with high penetration of wind power. IEEE Trans on Sustainable Energy, 5(3), pp.896-906.

[6] Ahadi, A., Ghadimi, N., Mirabbasi, D., 2014. Reliability assessment for components of large scale photovoltaic systems. Journal of Power Sources, 264, pp.211-219.

[7] Yang, S., Bryant, A., Mawby, P., Xiang, D., Ran, L., Tavner, P., 2011. An industry-based survey of reliability in power electronic converters. IEEE Trans on Industry Applications, 47(3), pp.1441-1451.

[8] Adinolfi, G., Graditi, G., Siano, P. and Piccolo, A., 2015. Multiobjective optimal design of photovoltaic synchronous boost converters assessing efficiency, reliability, and cost savings. IEEE Trans on Industrial Informatics, 11(5), pp.1038-1048.

[9] Zhang, M. Wang, and W. Su, "Reliability Analysis of Power Systems Integrated with High-Penetration of Power Converters", IEEE Trans. on Power Systems, 2020.

[10] Peng, C., Lei, S., Hou, Y. and Wu, F., 2015. Uncertainty management in power system operation. CSEE Journal of Power and Energy Systems, 1(1), pp.28-35.

[11] Hasan, K.N., Preece, R. and Milanović, J.V., 2016. Priority ranking of critical uncertainties affecting small-disturbance stability using sensitivity analysis techniques. IEEE Trans on Power Systems, 32(4), pp.2629-2639.

[12] Preece, R. and Milanović, J.V., 2015. Assessing the applicability of uncertainty importance measures for power system studies. IEEE Trans on Power Systems, 31(3), pp.2076-2084.

[13] Gonzalez, A., Echavarren, F.M., Rouco, L. and Gomez, T., 2012. A sensitivities computation method for reconfiguration of radial networks. IEEE Trans on Power Systems, 27(3), pp.1294-1301.

[14] Tamp, F. and Ciufo, P., 2014. A sensitivity analysis toolkit for the simplification of MV distribution network voltage management. IEEE Trans on Smart Grid, 5(2), pp.559-568.

[15] Calderaro, V., Conio, G., Galdi, V., Massa, G. and Piccolo, A., 2013. Optimal decentralized voltage control for distribution systems with inverter-based distributed generators. IEEE Trans on Power Systems, 29(1), pp.230-241.

[16] Ni, F., Nijhuis, M., Nguyen, P.H. and Cobben, J.F., 2017. Variance-based global sensitivity analysis for power systems. IEEE Trans on Power Systems, 33(2), pp.1670-1682.

[17] De León-Aldaco, S.E., Calleja, H. and Alquicira, J.A., 2014. Reliability and mission profiles of photovoltaic systems: A FIDES approach. IEEE Trans on Power Electronics, 30(5), pp.2578-2586.

[18] Liu, H., Liu, Z., Liu, S., Liu, Y., Bin, J., Shi, F. and Dong, H., 2018. A nonlinear regression application via machine learning techniques for geomagnetic data reconstruction processing. IEEE Trans on Geoscience and Remote Sensing, 57(1), pp.128-140.

[19] Nava, N., Di Matteo, T. and Aste, T., 2018. Financial time series forecasting using empirical mode decomposition and support vector regression. Risks, 6(1), p.7.

[20] Wu, X., He, J., Yip, T. and Lu, N., 2016, July. A two-stage random forest method for short-term load forecasting. In 2016 IEEE Power and Energy Society General Meeting (PESGM) (pp. 1-5). IEEE.

[21] Hu, Z. and Mahadevan, S., 2019. Probability models for data-driven global sensitivity analysis. Reliability Engineering & System Safety, 187, pp.40-57.

[22] Lei, H. and Singh, C., 2016. Non-sequential Monte Carlo simulation for cyber-induced dependent failures in composite power system reliability evaluation. IEEE Trans on Power Systems, 32(2), pp.1064-1072.

[23] Delgarm, N., Sajadi, B., Azarbad, K. and Delgarm, S., 2018. Sensitivity analysis of building energy performance: a simulation-based approach using OFAT and variance-based sensitivity analysis methods. Journal of Building Engineering, 15, pp.181-193.

[24] Barrows, C., Bloom, A., Ehlen, A., Ikäheimo, J., Jorgenson, J., Krishnamurthy, D., Lau, J., McBennett, B., O'Connell, M., Preston, E. and Staid, A., 2019. The IEEE reliability test system: A proposed 2019 Update. IEEE Trans on Power Systems, 35(1), pp.119-127.

[25] Bilir, L., Imir, M., Devrim, Y. and Albostan, A., 2015. Seasonal and yearly wind speed distribution and wind power density analysis based on Weibull distribution function. international journal of hydrogen energy, 40(44), pp.15301-15310.

CHAPTER 4

Node Reliability Interdependencies and Causal Relation Investigation

4.1. Introduction

In this chapter, BN structure searching and scoring algorithms are utilized to identify critical nodes and investigate their reliability interdependencies for a power system under great converter penetration. As more converters are integrated into the system, reliability interactions among various converters will frequently emerge and consequently introduce system reliability concerns. However, reliability causal relations have rarely been explored and demonstrated in a clear manner. Therefore, BN structure learning is applied to visualize the proposed converter-based BN structure. Moreover, reliability interactions among different nodes are quantified through information entropy theory. Numerical case studies illustrate the causal reliability relations among various nodes while considering the reliability of all integrated converters. Critical nodes are identified such that system operators can improve the converter maintenance scheduling.

With the deepening integration of renewable energy sources (RES), the complexity of evaluating a power system's reliability has been increasing progressively in recent years. Compared to traditional power generation, for example, RESs are easily influenced by ambient conditions. Intermittency of an RES may cause uncertainty issues in system operation and weaken the system's reliability [2]-[6]. On the other hand, the power electronic converter is essentially integrated and performs the underpinning role of power conversion between RES/battery storage and the main system. Moving toward one hundred percent RES integration

has further intensified the importance of analyzing the reliability performance of converter-penetrated power systems.

Table 7 provides a brief literature summary on both component and system level reliability analysis. From the component perspective, identifying critical components in a power system has raised much research attention [7]-[13]. Various components, including transmission lines [7], transformers [8]-[9], energy storage systems [9] and load points [11], have been considered most critical when conducting system reliability evaluation. However, converter reliability has rarely been considered as one of the potential causes of system failures in the existing literature. Converter reliability impacts on the overall system reliability have spurred only limited research attention [19]-0. The authors in [19] considered the power converter one of the most frequently failed components in various applications and thus that increasing converter implementation will have great impact on system reliability performance. A DC-DC converter reliability model was formulated in [9] in evaluating the reliability of an energy storage system, but its impact on other components' reliability was not investigated and different types of converters were not considered. The authors in 0 provided a reliability ranking for multiple converters based on their impacts on system reliability, but the reliability relations among different converters were not explored.

Table 7: Literature summary of reliability analysis

Research Areas	Ref.	Research Focus	Consider Converter Reliability?	Reliability Quantification
Component	[7]	Transmission lines	No	Customer Interruption Cost
	[8], [9]	Transformer	No	EENS
	[9]	Battery Systems	Yes (DC-DC converter only)	Failure rate
	[11]	Critical loads	No	Cumulative service time
	[13]	RES	No	Cost of Energy
System	[14]	Structural improvement	No	Node clusters
	[15]	Electric/Information system interdependency	No	Node coupling rate
	[16]- [18]	Cascading failure	No	Failure probability

From the system-level perspective, illustrating a system network through a graph that is composed of many nodes with various mutual relations [15] can clearly demonstrate the risk points such that the system reliability can be improved. Today's power system network is clearly amenable to such description. Reference [14] utilized complex network theory to conduct node clustering and visualized the system network augmentation. The authors in [16] investigated various scenarios of system cascading failure, with all failed load points graphically presented. In terms of the system reliability correlation, the authors in [15] claimed that there is a clear reliability interdependency between the power system and the information and communication technology (ICT) systems. However, the other type of interaction, namely, the causal relation/connectivity between components has rarely been investigated in the existing literature. A signal directed graph was used in 0 to describe a system with a graphical representation of causal relations amongst variables that can be applied to find fault propagation paths and explain the causes of a fault. However, this method was greatly dependent on human effort and only suitable for linear models. Complex network theory was used in 0 for detecting variable correlations, but its electrical explanation of each node was not straightforward. A more universal approach should be utilized if those interactions and the system itself have strong nonlinearity.

This chapter mainly focuses on learning the skeleton structure and investigating the causal reliability relations among the integrated converters of a converter-penetrated power system. Fig. 15 illustrates an overview of the proposed reliability evaluation framework. The electric power system is implemented with multiple renewable generators such as wind energy and solar power sources. Specific power converters are integrated with each RES to properly convert the generated renewable power and transfer it to the main grid. As more RESs and converters penetrate the system, it is technically difficult and less efficient to observe the state of every component when

evaluating/analyzing the system reliability. However, converters are greatly distributed across the system and as mentioned before, are one of the most vulnerable components/sub-systems in a power system. Therefore, we utilize both BN 0 structure learning algorithms and information entropy theory 0 to construct a converter-based BN structure where:

- Each node considers the reliability of multiple components, including the generator, transformer and especially, the reliability of the converter connected on it. Probabilistic data of each converter's reliability are collected, and we apply Shannon entropy H to quantify the uncertainty of each node.
- Each oriented edge refers to the causal reliability relation between two nodes. The existence of each edge is addressed by calculating mutual information and we determine the edge orientation by calculating transfer entropy such that each causal reliability relation between two nodes can be quantified.
- Those nodes that have high uncertainty and wide influential relations on other nodes are identified as critical to help the system operator optimize schedule prior maintenance/inspections.

It is worth noting that the generated converter-based BN structure is unique from the original physical power system network. Information such as the level of uncertainty on each node, the quantified causal relations among multiple nodes can only be revealed under the generated BN structure instead of the original physical network. We aim to enhance the importance of considering power converters reliability effects and causal interactions when evaluating the reliability of today's power system. The proposed BN structure demonstrates these focuses and can perform as an evaluation enrichment compared to existing system reliability assessment.

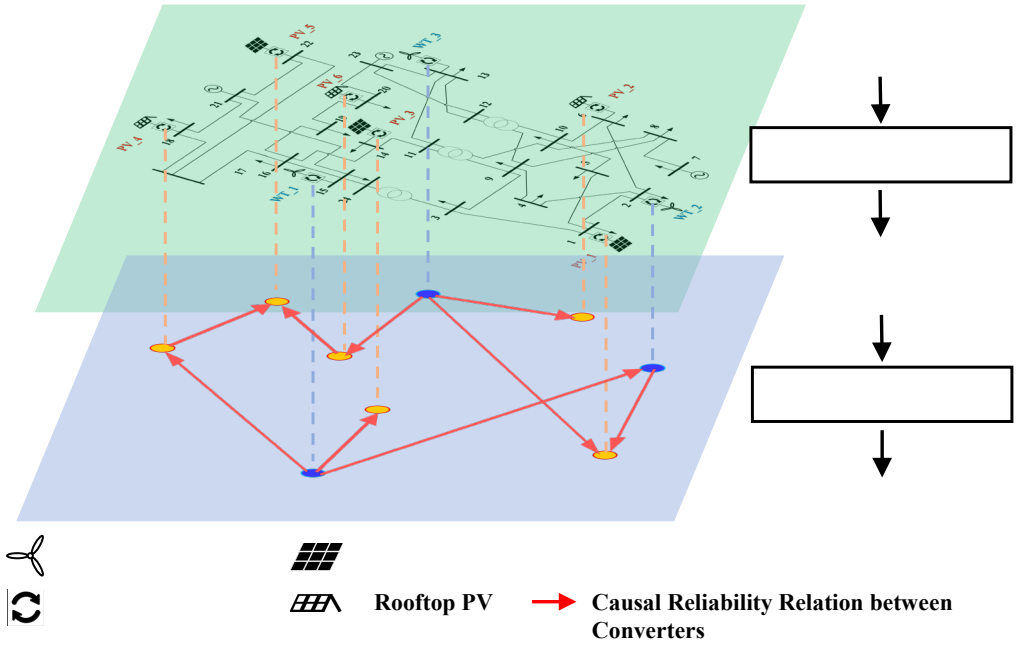

Figure 15. An overview of the proposed reliability evaluation framework

This chapter has the following contributions:

1) We propose a converter-based BN that performs as the skeleton structure of a converter-penetrated power system and utilizes BN structure learning to visualize identified causal relations among different nodes. The reliability of each power converter is enhanced during the learning procedure. As more RESs and energy storage systems are integrated into the system, power converters are heavily distributed and play a very important role in today's power system. Their importance should be further enhanced.

2) For the first time, we integrate information entropy theory to quantify the uncertainty of each node and each causal relation such that the criticality/vulnerability of all nodes can be provided for system operators to better schedule operations and maintenance.

3) We utilize BN structure learning and transfer entropy estimation methods collaboratively to illustrate comprehensively the causality among various nodes. The

reliability interdependency and failure propagation are clearly illustrated to enrich the understanding of the reliability performance of a converter-penetrated power system.

The rest of this chapter is organized as follows. First, the concept of BN structure learning and information entropy concepts are presented. Subsection 4.3 provides the reliability modeling of WT/PV converters and an overview of the proposed system reliability evaluation framework. In Subsection 4.4, several case studies are conducted on a modified IEEE 24-bus RTS to demonstrate the effectiveness of the proposed methodology. Conclusions are summarized in Subsection 4.5.

4.2. Transfer Entropy-integrated BN Structure Learning

In this work, Bayesian network (BN) structure learning and transfer entropy are collaboratively applied to the proposed converter-penetrated power system for investigating the causal relationships among different converter reliability performance. Basic concepts and the proposed transfer entropy-integrated BN structure learning are introduced in this section.

4.2.1. BN Structure Learning

The BN has been proven to be a versatile tool in various fields 0. It has been considered one of the most effective and classic graphical models in power system reliability studies as well as providing probabilistic information and inferences via a directed acyclic graph (DAG). The proposed BN structure consists of three components: (V, E, Θ), where a set of nodes $V = \{X_1, X_2, \dots, X_N\}$ represent N power converters' reliability, and we can assess the reliability of each converter from system Monte Carlo simulation and observe the physical/thermal behavior of each converter. As more power converters are integrated into the power system, the scale of V will

increase; E denotes the set of edges. Each element e_{ij} in E represents an edge directed from X_i to X_j, which represents the causal relation between two converters' reliability performance; Each element $\theta_i \in \Theta$ denotes the conditional probability distributions of the converter reliability X_i.

4.2.2. Search & Score Functions

Currently, search & score-based methods are usually applied to construct BN structures 0-0. Search algorithms together with several scoring functions are applied to evaluate the goodness of each explored feasible BN structure. The objective of utilizing this method is to find a DAG which maximizes the selected scoring function. The search algorithm determines the structure learning efficiency while the scoring function affects the learning accuracy.

With a given data set D, the problem of BN structure learning from D can be described as follows: finding a DAG (G) which is the best fit for the data set D in some senses. The scoring function is applied to evaluate the fitness of a candidate DAG to D. The scoring criteria is shown in equation (4.1) where the value of $score(D)$ can be determined by the data set D.

$$score(G, D) = score(G|D)score(D) \tag{4.1}$$

$$G^* = \arg\max_{G \in G^n} score(G|D) \tag{4.2}$$

Equation (4.2) states that the objective is to find the optimal BN structure G^* where G^n is the set of all feasible DAGs.

The BIC scoring function was proposed based on an assumption that samples are subject to independence and an identical distribution. In BIC, the fitness of a DAG for the given data set D is evaluated based on log likelihood. The formula of the BIC scoring function is shown in equation (4.3), where N is the number of variables in the DAG; P_i is the number of possible

configurations of the parent set $Pa_G(X_i)$ of X_i; S_i is the number of states of the variable X_i; m_{ijk} is the number of observations in the data set D where the variable X_i is under the state k and the parent set is in the jth configuration; $\theta_{ijk} = \frac{m_{ijk}}{m_{ij}}$ $(0 \leq \theta_{ijk} \leq 1, \sum_k \theta_{ijk} = 1\,, m_{ij} = \sum_{k=1}^{r_i} m_{ijk})$ is the likelihood conditional probability; m is the number of samples in D. The first item of this BIC scoring is the log likelihood, and the second item performs as a penalty function to avoid overfitting.

$$BIC(G|D) = \sum_{i=1}^{X_N} \sum_{j=1}^{P_i} \sum_{k=1}^{S_i} m_{ijk} \log \theta_{ijk} - \frac{1}{2} \sum_{i=1}^{X_N} P_i (S_i - 1) \log m \tag{4.3}$$

Another scoring function named BDe is proposed based on Bayesian statistics and is shown in equation (4.4), where $\alpha_{ij} = \sum_{k=1}^{S_i} \alpha_{ijk}$ and α_{ijk} describes the prior distribution. The main principle of BDe is to find a DAG that can maximize the posterior probability considering both data characteristics and prior knowledge.

$$BDe(G|D) = \sum_{i=1}^{X_N} \sum_{j=1}^{P_i} [\log \frac{\Gamma(\alpha_{ij})}{\Gamma(\alpha_{ij} + m_{ij})} + \sum_{k=1}^{S_i} \log \frac{\Gamma(\alpha_{ijk} + m_{ijk})}{\Gamma(\alpha_{ijk})}] \tag{4.4}$$

In terms of the search algorithm, however, searching the optimal network structure is a non-deterministic polynomial-hard problem. Thus, widely used score-based algorithms, namely K2 and MMHC algorithms, are selected as the search strategy.

4.2.3. Transfer Entropy

Information entropy is a well-known signal processing technique, and it has recently proved its suitability for evaluating complex system reliability such as fault detection 0 and uncertainty quantification 0. The concept of information entropy was proposed as a measure of information and uncertainty of a variable. Suppose there are two variables A and B and their states

(a_j^t, b_k^t) are observed at each hour t. An entropy rate h_1 is defined as the amount of additional information required to represent the value of the next observation of A:

$$h_{\mathrm{I}} = -\sum_{j=1}^{S_j}\sum_{k=1}^{S_k} P(a_j^{t+1}, a_j^t, b_k^t)\log P(a_j^{t+1}|a_j^t, b_k^t) \tag{4.5}$$

On the other hand, if a_j^{t+1} is independent of the current observation b_k^t, the entropy rate is calculated as in equation (4.6):

$$h_{\mathrm{II}} = -\sum_{j=1}^{S_j}\sum_{k=1}^{S_k} P(a_j^{t+1}, a_j^t, b_k^t)\log P(a_j^{t+1}|a_j^t) \tag{4.6}$$

In general, the quantity of h_{I} represents the entropy rate when the current state of B can affect the future state of A, while h_2 assumes the future state of A is independent from the current state of B.

Thus, the transfer entropy is defined as the deviation from independence of the state transition of an information destination B from the previous state of an information source A. When the observation delay is 1 hour, the transfer entropy can be calculated by (4.7):

$$T_{A\to B}(j,k) = h_{\mathrm{II}} - h_{\mathrm{I}} = \sum_{j=1}^{S_j}\sum_{k=1}^{S_k} P\left(a_j^{t+1}, a_j^t, b_k^t\right)\left|\log\left(\frac{P(a_j^{t+1}|a_j^t, b_k^t)}{P(a_j^{t+1}|a_j^t)}\right)\right. \tag{4.7}$$

where t is the time index, a_j^t and b_k^t indicate the jth and kth state of variable A and B at time t, respectively.

It is assumed in both h_{I} and h_{II} that a_j^{t+1} can be influenced by a_j^t (i.e., the future state of A is influenced by its current state). The value of $T_{A\to B}$ quantifies the information difference between "assume b_k^t can affect a_j^{t+1}" and "b_k^t is independent from a_j^{t+1}". In this way, $T_{A\to B}$ indicates the causal relation between A and B. This formulation is a directional and dynamic

measure of information transfer from A to B. It shows that the uncertainty changes of a_j^{t+1} between given conditions of b_k^t and unknown b_k^t can be described using transfer entropy. In other words, the information transferred from b_k^t to a_j^{t+1} can be represented by transfer entropy. The transfer entropy formulation is a generalization of the entropy rate to more than one variable. It is worth noting that transfer entropy remains a measure of the observed correlation rather than of the direct effect between variables.

4.2.4. Transfer Entropy-integrated Scoring Function

The causal relations among multiple converters can be complicated since the reliability of each converter can be corelated by many other converters' performance and vice versa. For example, A WT converter failure would terminate the power conversion and the power generated from this WT cannot be transferred into the main grid and also the load side. To supplement power for the affected area, either the battery storage system (BSS) or other available power generations will be required to provide more power compared to their regular power contributions. As a result, this kind of burden will affect the reliability performance of those converters connected with BSS and other renewable generators.

As stated in subsection A.2, $Pa_G(X_i)$ refers to the parent set of X_i, which means each element in $Pa_G(X_i)$ can potentially affect the reliability of X_i. Thus, multiple edges would exist and all of them would be directed to X_i in the DAG. Moreover, since transfer entropy quantifies the information exchange, it can be utilized as a weighting index on each directed edge and describes the degree of each causal relation. Thus, the total transfer entropy from $Pa_G(X_i)$ to X_i is described in equation (4.8), which is used to quantify the reliability causality between each converter X_i and its parent set $Pa_G(X_i)$.

$$T_{Pa_G(Xi)\to X_i}(j,k)=\sum_{j=1}^{S_j}\sum_{k=1}^{S_k}P\left(x_j^{t+1},x_j^t,Pa_G(X_i)_k^t\right)|\log\left(\frac{P\left(x_j^{t+1}\middle|x_j^t,Pa_G(X_i)_k^t\right)}{P\left(x_j^{t+1}\middle|x_j^t\right)}\right) \tag{4.8}$$

In terms of the scoring function, as shown in equation (3), the log likelihood term ($\sum_{i=1}^{N}\sum_{j=1}^{P_i}\sum_{k=1}^{S_i}m_{ijk}\log\theta_{ijk}$) in the BIC scoring function indicates the fitness between the learned DAG and the given data set D, which can be rewritten in equation (4.9), where the term within the square bracket represents the entropy when $Pa_G(X_i)$ is given, and can be replaced by h_I in equation (4.5). Thus, the log likelihood term in the scoring function can be determined during the transfer entropy calculation.

$$\begin{aligned} log\ likelihood(G|D)&=\sum_{i=1}^{X_N}\sum_{j=1}^{P_i}\sum_{k=1}^{S_i}m_{ijk}\log\theta_{ijk}=m\sum_{i=1}^{X_N}\sum_{j=1}^{P_i}\sum_{k=1}^{S_i}\frac{1}{m}m_{ijk}\log(\frac{m_{ijk}}{m_{ij}})\\ &=m\sum_{i=1}^{X_N}[\sum_{j=1}^{P_i}\sum_{k=1}^{S_i}P(X_i,Pa_G(X_i))\log P(X_i|Pa_G(X_i))]=-mh_I \end{aligned} \tag{4.9}$$

In general, each transfer entropy value is calculated to quantify the causal relation between each element of $Pa_G(X_i)$ and X_i. The accumulated transfer entropy $T_{Pa_G(Xi)\to X_i}$ which helps determine the log likelihood function, can be calculated after exploring all elements in $Pa_G(X_i)$. The BIC scoring function is then utilized to evaluate the fitness of each feasible structure.

4.3. An Overview of the Proposed Framework

An overview of the proposed reliability evaluation framework is illustrated in Fig.16. In the proposed reliability evaluation framework, the first step is to construct an undirected structure, and a set of training data is required. The data set consists of state vectors $T=\{X_i,\dots,X_N,L_1,\dots,L_{tl},LOLE\}$, where X_i denotes the ith converter reliability. L_i is the state of ith transmission line, and its value equals one if it is under a failed state; otherwise, it is zero. $LOLE$

represents the typical reliability indicator, namely, loss of load expectation in the power system. N, tl are the number of integrated converters and transmission lines, respectively. The hourly-based input data such as wind angle, wind speed, ambient temperature and solar radiance are applied to calculate the reliability of WT/PV converter while reliability data of other components are also collected. State sampling of Monte Carlo simulation 0 is used to determine the state of each component in the system. We summarize the steps of generating the training data as follows: First, the reliability state of each component is determined by generating uniformly distributed random numbers between 0 and 1, which is further compared with the component reliability or forced outage rate (FOR). If the sampled value is smaller than the FOR value, the component is under an outage state. Otherwise, the component is under a normal state. After all components' states are determined, the overall system can be under a normal/contingency state and the value of $LOLE$ can be calculated. As introduced in Section 4.2, BN structure searching algorithms and scoring functions are applied to generate a BN from the original electrical network.

Meanwhile, given the probability distribution of each converter reliability, the Shannon entropy $H(X_i)$ can be calculated to quantify the uncertainty level of each X_i. Based on the training data and expert knowledge, values of mutual information are calculated to determine the existence of edges in the structure.

To investigate the causal relation between converter reliabilities, transfer entropy is further calculated on each edge. It is worth noting that both $T_{X\to Y}$ and $T_{Y\to X}$ should be calculated in terms of variable X and Y. In general, it is asymmetry between $T_{X\to Y}$ and $T_{Y\to X}$. If $T_{X\to Y} \gg T_{Y\to X}$, then the causal relation is considered as: $X \to Y$, which means that given the information of X will greatly help predict the reliability performance of Y at that moment, and vice versa. Even X and Y are greatly coupled in reality and they affect each other throughout a year. At a certain time t,

however, the causal relation is considered uni-directional if the values of $T_{X\to Y}$ and $T_{Y\to X}$ are not equal.

Since $H(X)$ denotes the uncertainty of each converter and TE explores all causal relations among all converters, a reliability criticality of converters can be generated by comprehensive comparison/analysis of these entropy values. The vulnerability/criticality of each converter is then determined. Identified critical converters should have priority to have maintenance or get equipped with a reliability sensor such that their reliability information can be fully observed/monitored. The overall system entropy, i.e., the system uncertainty, is further reduced.

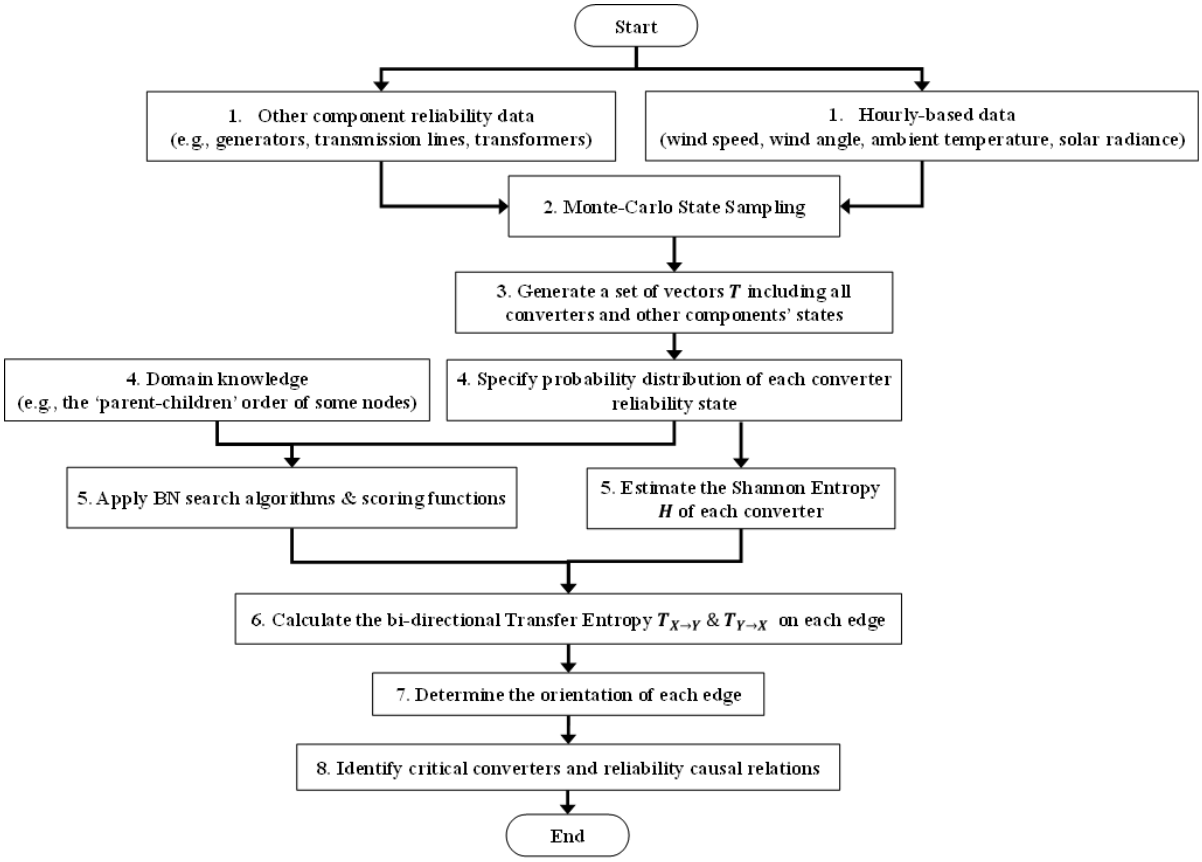

Figure 16. An overview of the proposed framework

4.4. Numerical Analysis

In this section, the proposed reliability evaluation framework is validated on the modified 24-bus IEEE reliability test system (RTS). The computations, including MC simulations, are performed in Matlab 2020a on an Intel Core at 2.90GHz with 16 GB RAM. BN structure learning is realized through Bayes Net Toolbox 0 and Python pgmpy 0. A Matlab toolbox called cTE 0 is modified for the transfer entropy estimations. Fig.17 presents the modified 24-bus IEEE RTS network. RTS was first published in 1979 as a benchmark for testing various reliability analysis methods.

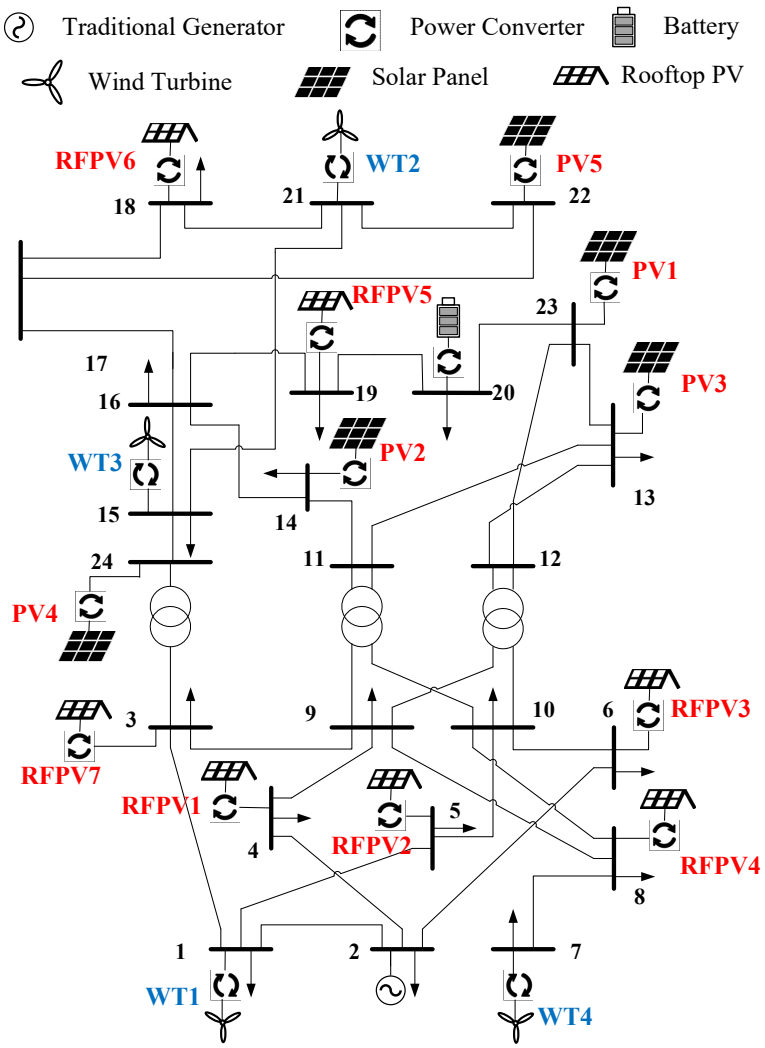

Figure 17. The modified 24-bus IEEE RTS network

4.4.1. Information about the System Physical Network

In all case studies, we use the updated version of RTS data 0 where some conventional oil-fueled generating units were replaced by RESs and energy storage systems. Four wind turbines (WT), five photovoltaic (PV) generators and seven rooftop PVs (RFPV) have been added to the system. Table 8, 9 and 10 provide all RES locations and capacity information.

Table 8: Location and capacity information for WT converters

No. of WT	Bus ID	Capacity (MW)
1	1	148.3
2	21	217.5
3	15	155.0
4	7	191.1

Table 9: Location and capacity information for PV converters

No. of PV	Bus ID	Capacity (MW)
1	23	51.6
2	14	51.6
3	13	92.7
4	24	49.7
5	22	51.7

Table 10: Location and capacity information for RFPV converters

No. of RFPV	Bus ID	Capacity (MW)
1	4	27.0
2	5	28.2
3	6	9.7
4	8	11.2
5	19	10.3
6	18	27.2
7	3	9.4

4.4.2. BN Structure Learning Results

As introduced in previous subsections, the Shannon entropy represents the level of uncertainty on each variable and transfer entropy quantifies the information transferred between two variables. Since each converter reliability performs as a variable, and any converter reliability

performance can be passively affected by or can affect other converters, we not only estimate the Shannon entropy but also calculate the value of delivered and received transfer entropy of each converter to comprehensively evaluate its importance/criticality.

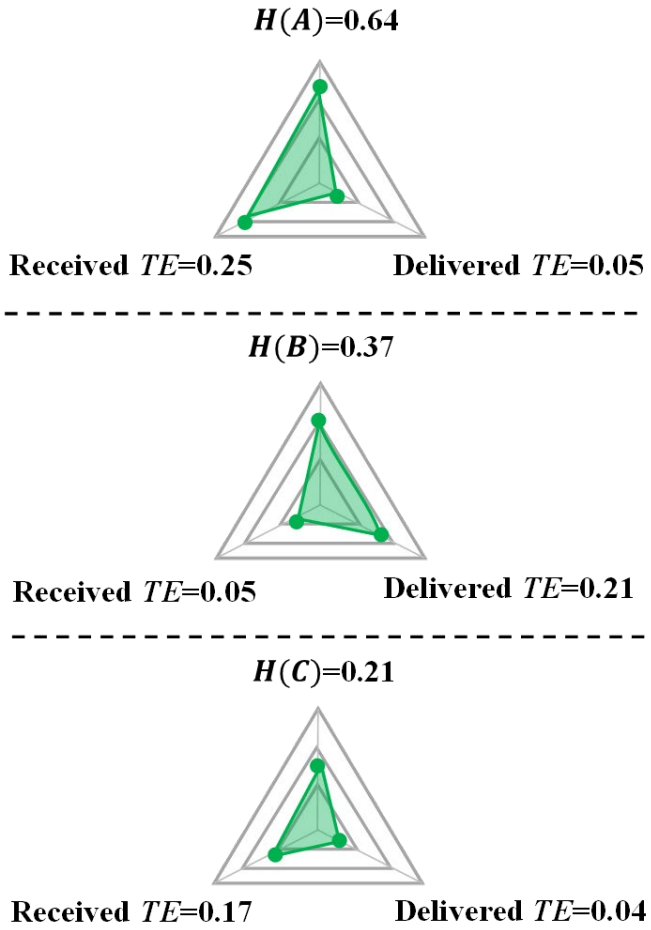

Figure 18. Calculated entropy values of each variable

For example, as shown in Fig.18, in a network with three variables $\{A, B, C\}$, we consider the Shannon entropy of all variables $\{H(A), H(B), H(C)\}$ to quantify the level uncertainty of each variable. Since each variable x will normally deliver/receive some information to/from another variable y, namely, both $T_{x\to y}$ and $T_{y\to x}$ will exist, we also calculate these two transfer entropy values to determine the orientation of each causal relation. As shown in Fig.19, since the variable B delivers more information to A and does not receive much information from A, we can conclude

that the variable B tends to affect A rather than gets influenced by it. Therefore, the edge orientation between A and B is $B \rightarrow A$.

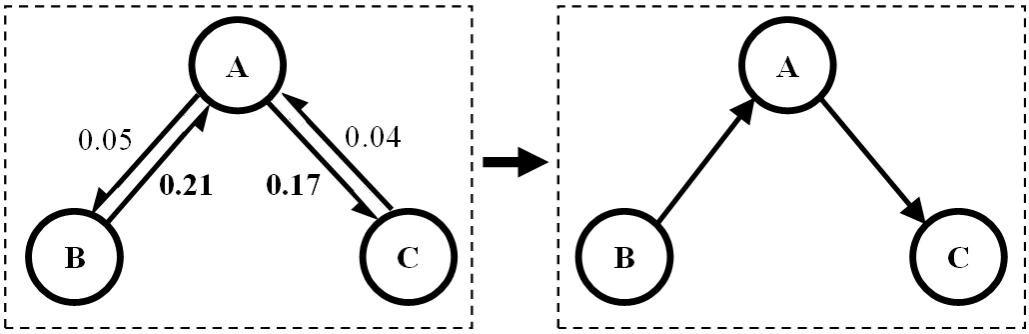

Figure 19. An example of determining the edge orientation

In the proposed network, some causal relations (e.g., node $1 \rightarrow 2$, $6 \rightarrow 10$, $7 \rightarrow 8$ and $21 \rightarrow 18$) are obvious by applying prior knowledge. The learning results based on integrated three scoring functions of these assumptions are listed in Table 11. "Y" indicates that the causal relation between two nodes is correctly learned while "N" indicates the causal relation is not learned/considered not significant. The proposed function learned all four causal relations correctly while one or two relation was not detected by BIC and BDe, respectively.

Table 11: Learning comparisons among different scoring functions

Causal relations	$\mathbf{1 \rightarrow 2}$	$\mathbf{6 \rightarrow 10}$	$\mathbf{7 \rightarrow 8}$	$\mathbf{21 \rightarrow 18}$
BDe	Y	N	Y	N
BIC	Y	Y	Y	N
Transfer entropy-integrated BIC	Y	Y	Y	Y

Fig.20 presents the BN structure learned from the original 24-bus electrical network, where each node represents the bus reliability, considering the reliability of generator, integrated converter, load and other components, and each directed edge represents the reliability causal relation between two nodes. K2 and MMHC algorithm are applied as the searching strategies to explore the BN structure. Prior knowledge such as bus generation and load information, converter FOR 0-0, and MC simulation data is used to help generate a set of node orders. To avoid structure

overfitting and remove weak connections, the threshold value of mutual information is adjusted to 0.10. It can be observed that most nodes have multiple causal relations (edges). For example, node 5 has two edges which indicate its reliability performance can potentially affect the performance of node 10 and can be influenced by the reliability performance of node 1.

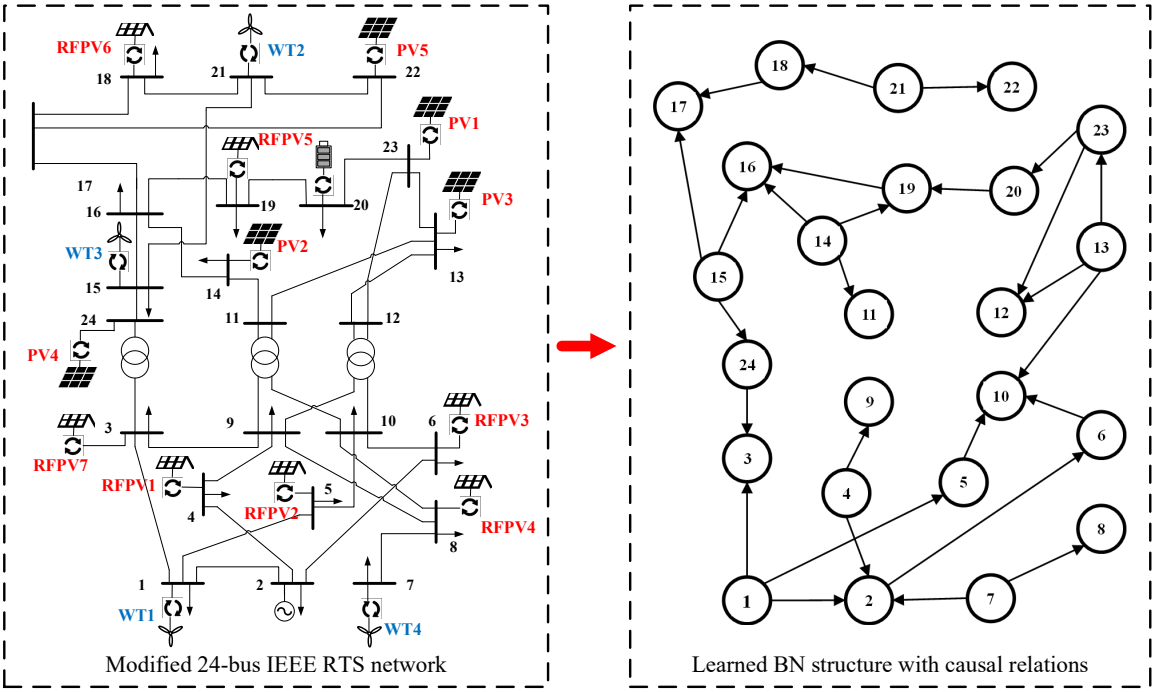

Figure 20. The learned BN structure based on the proposed scoring function
(Left figure: Node - bus, edge – physical connection Right figure: Node – reliability of each bus, edge – causal relation)

It is not a one-to-one mapping between the original physical RTS network and the learned BN structure. It is worth noting that this is a one-to-one mapping between the original physical network and the learned BN structure. For example, there exists a physical connection between node 9 and 11, but in the learned BN structure, there is no causal relation between these two nodes.

Critical nodes are marked with solid red such as {1, 13, 14, 15} in Fig.21 because all orientations of their edges target toward other nodes, which indicate their reliability can potentially affect the reliability performance on their related nodes. Another set of nodes with red diagonal stripes (e.g., node 10 and 16) indicate that these nodes can be easily influenced. These nodes

receive more information than deliver it such that the reliability on these nodes can be greatly determined by the reliability performance of other nodes.

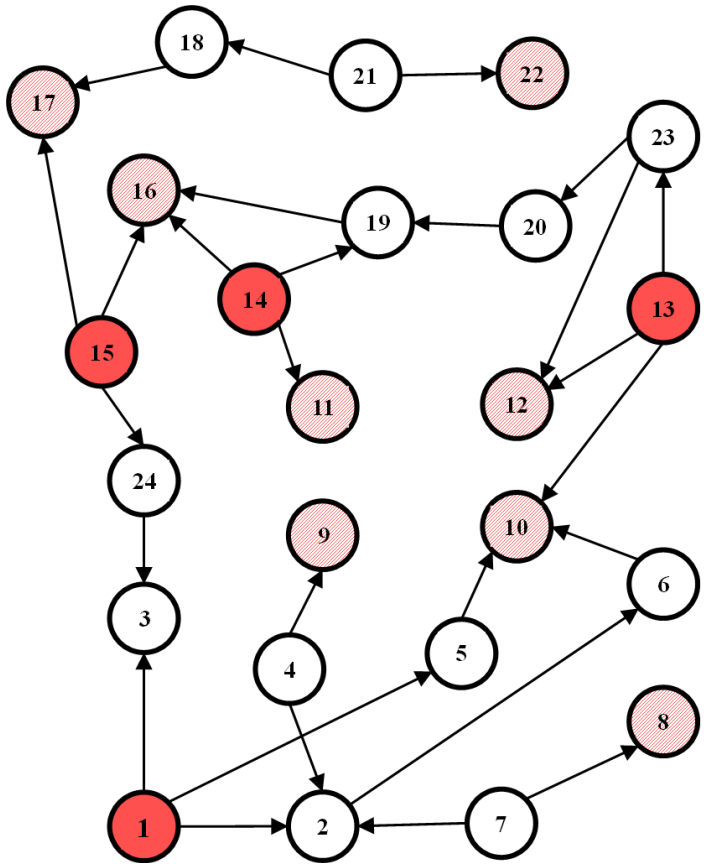

Figure 21. Illustrated critical nodes in the BN structure

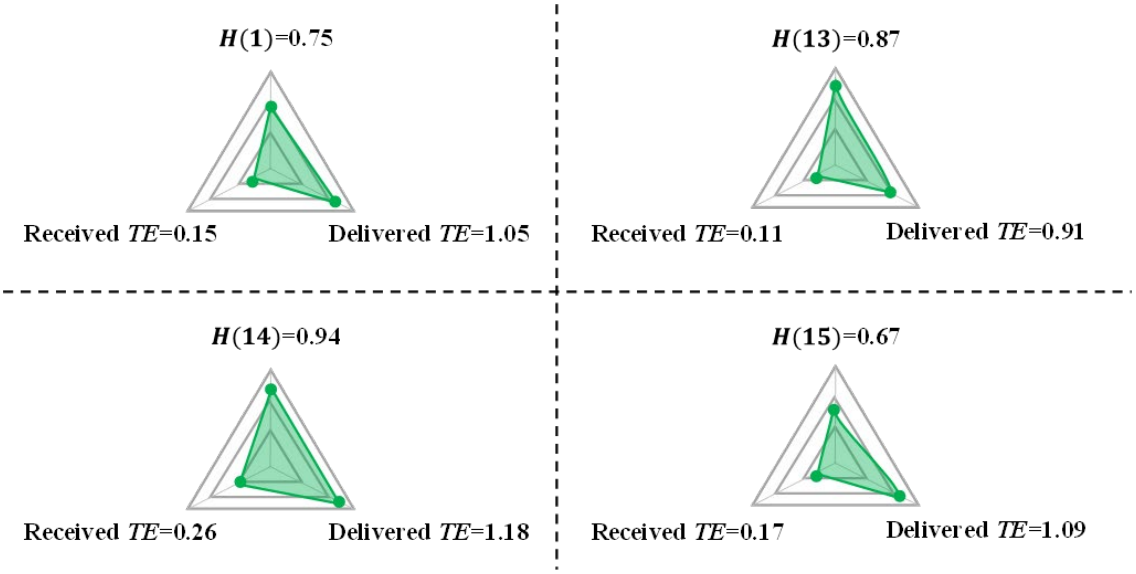

Figure 22. Calculated Shannon and transfer entropy (TE) on critical nodes

Fig. 22 illustrates the calculated entropy values of critical nodes. The Shannon entropy H on node 1, 13, 14 and 15 is relatively high which indicates the uncertainty on these nodes is under a high level. The delivered transfer entropy indicates how much information is delivered to other related nodes. Therefore, these nodes are considered more impactful/critical, and moreover, all their edges direct towards other nodes, namely, their reliability performance will probably impact multiple other nodes.

4.4.3. Outages on Critical Nodes and Their Propagation Areas

Critical nodes such as 1, 13, 14, 15 are identified in the previous subsection and they are more likely to impact the reliability of other nodes. For example, if a converter failure happened on node 1, the performance of node 2, 3 and 5 will probably be influenced. However, this does not guarantee that the outage area is limited to these four nodes since nodes {2, 3, 5} also have causal relations with other nodes. Similarly, node 10, for example, can be easily influenced but not limited to {5, 6, 13} since cascading failure can possibly happen.

Node sensitivity refers to how the reliability degree of other nodes are influenced if one node reliability has a small change. The sensitivity analysis is conducted on each critical node and the largest propagation area is presented in fig. 23 and fig.24. The dotted square on the node indicates a small reliability change is applied while the grey marks the influenced nodes. For example, a small increase on the failure rate of node 13 will increase the outage probability on nodes {10, 12, 23, 20, 19, 16}. It can be observed that the identified causal relations basically match with the failure propagation area and either node 10 or 16 is affected in all analyzed results.

It is worth noting that the learned BN structure is generated and different from the original 24-bus electrical network. The electrical network shows the physical connections while the BN

structure illustrates the reliability causal relations among nodes. Since each node uncertainty is quantified by Shannon entropy (the level of uncertainty) and each causal relation is evaluated by transfer entropy, namely, the reliability information transferred between nodes, the failure propagation includes events such as cyber-attacks. Therefore, these analyzed propagation areas and quantified uncertainty information cannot be revealed by the original electrical network but are uniquely generated from the BN structure.

As the scale of the power system increases, it becomes more time consuming and complicated to conduct failure test on each node and estimate the affected area. The proposed BN structure identifies critical nodes by learning causal relations with entropy quantification, such that the failure testing efficiency is improved, especially when the maintenance schedule is tight, or resource is limited.

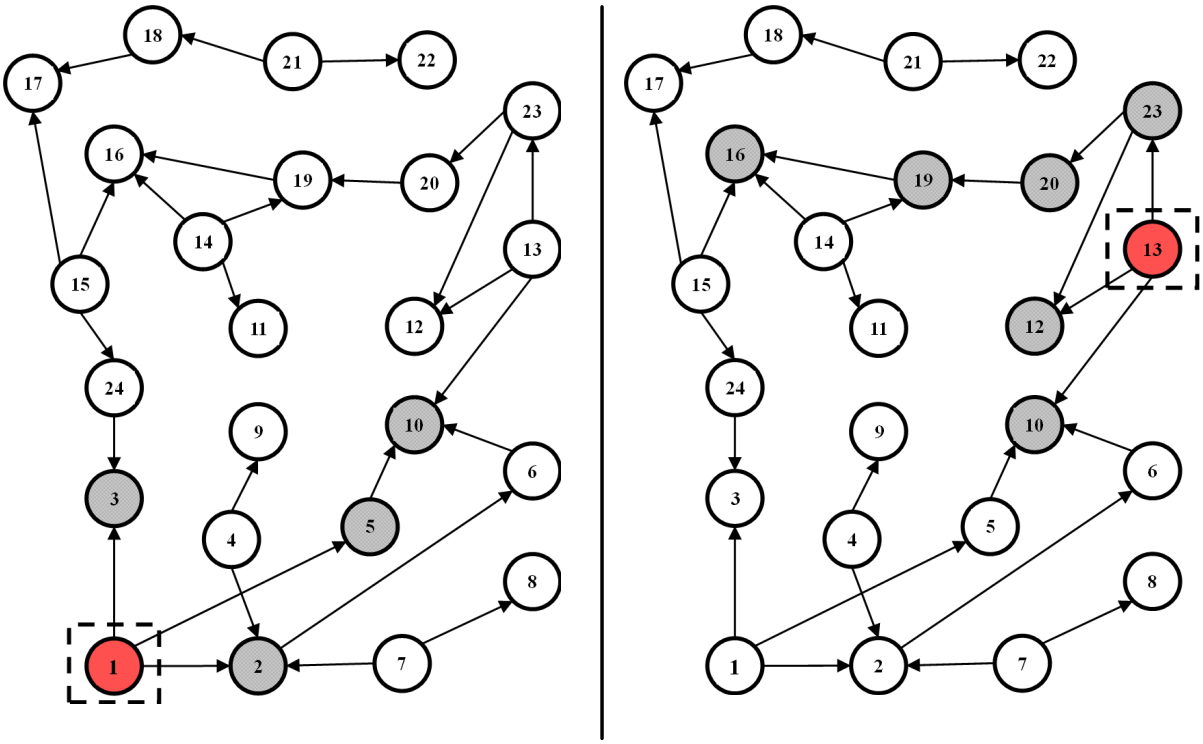

Figure 23. The failure propagation area when outage happened on node 1 and 13

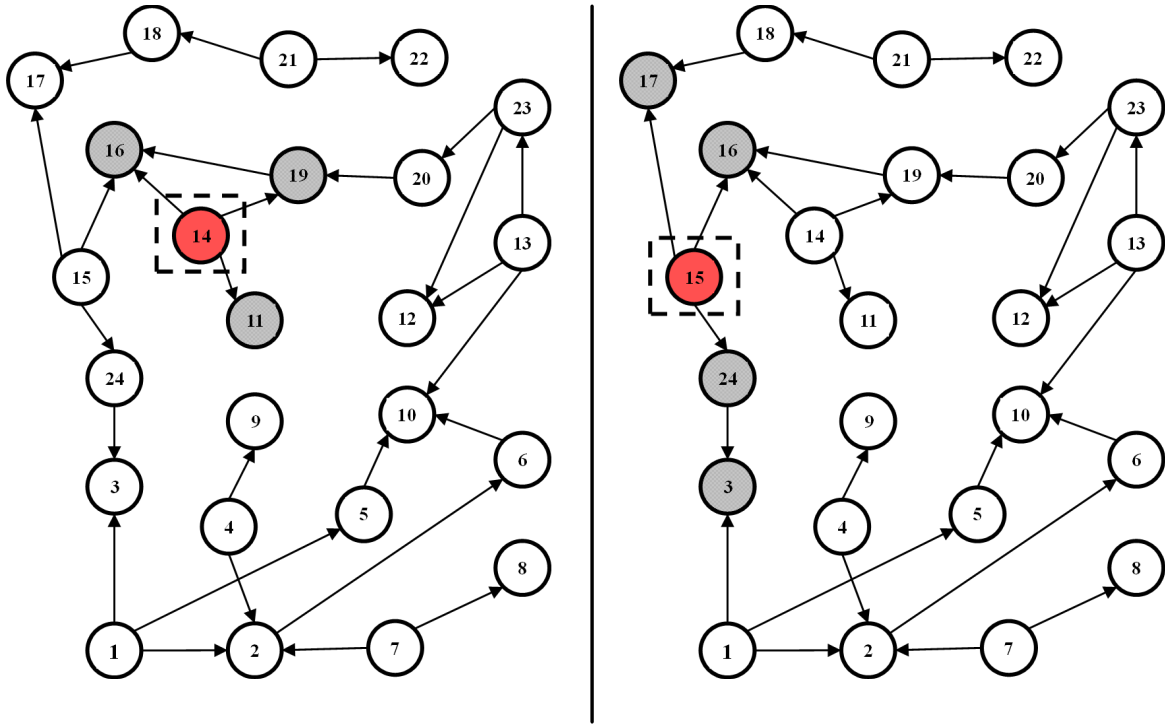

Figure 24. The failure propagation area when outage happened on node 14 and 15

4.5. Conclusions

This chapter has presented a framework to enhance the reliability analysis of a converter-penetrated power system. A BN structure is generated by utilizing BN structure search and scoring algorithms, which can be beneficial for illustrating the causal relations in complex system structures. Not only the uncertainty of each converter, but also various reliability causal relations among converters are explored and quantified through information entropy. Numerical analysis has demonstrated the reliability causal relations among different nodes and has evaluated the criticality/vulnerability of all nodes for system operators to improve the maintenance scheduling. Future research will focus on improving computational costs of complex system BN structure learning. Moreover, optimal placement can be investigated given a limited number of reliability sensors such that a detailed maintenance strategy could be generated.

4.6. References

[1] Hakimi, S.M. and Moghaddas-Tafreshi, S.M., 2014. Optimal planning of a smart microgrid including demand response and intermittent renewable energy resources. *IEEE Transactions on Smart Grid*, *5*(6), pp.2889-2900.

[2] Su, W., Wang, J. and Roh, J., 2013. Stochastic energy scheduling in microgrids with intermittent renewable energy resources. *IEEE Transactions on Smart grid*, *5*(4), pp.1876-1883.

[3] Aflaki, S. and Netessine, S., 2017. Strategic investment in renewable energy sources: The effect of supply intermittency. *Manufacturing & Service Operations Management*, *19*(3), pp.489-507.

[4] Hamoud, G.A., 2008, May. Assessment of transmission system component criticality in the de-regulated electricity market. In *Proceedings of the 10th International Conference on Probablistic Methods Applied to Power Systems* (pp. 1-8). IEEE.

[5] Awadallah, S.K., Milanović, J.V. and Jarman, P.N., 2014. The influence of modeling transformer age related failures on system reliability. *IEEE Transactions on Power Systems*, *30*(2), pp.970-979.

[6] Awadallah, S.K., Milanović, J.V. and Jarman, P.N., 2015. Quantification of uncertainty in end-of-life failure models of power transformers for transmission systems reliability studies. *IEEE Transactions on Power Systems*, *31*(5), pp.4047-4056.

[7] Liu, M., Li, W., Wang, C., Polis, M.P. and Li, J., 2016. Reliability evaluation of large-scale battery energy storage systems. *IEEE Transactions on Smart Grid*, *8*(6), pp.2733-2743.

[8] Xu, Y., Liu, C.C., Schneider, K.P., Tuffner, F.K. and Ton, D.T., 2016. Microgrids for service restoration to critical load in a resilient distribution system. *IEEE Transactions on Smart Grid*, *9*(1), pp.426-437.

[9] Blaabjerg, F., Yang, Y., Ma, K. and Wang, X., 2015, November. Power electronics-the key technology for renewable energy system integration. In *2015 International Conference on Renewable Energy Research and Applications (ICRERA)* (pp. 1618-1626). IEEE.

[10] Wang, J., Yu, X. and Stone, L., 2016. Effective augmentation of complex networks. *Scientific reports*, *6*(1), pp.1-9.

[11] Tøndel, I.A., Foros, J., Kilskar, S.S., Hokstad, P. and Jaatun, M.G., 2018. Interdependencies and reliability in the combined ICT and power system: An overview of current research. *Applied computing and informatics*, *14*(1), pp.17-27.

[12] Thapa, M., Espejo-Uribe, J. and Pournaras, E., 2019. Measuring network reliability and repairability against cascading failures. *Journal of Intelligent Information Systems*, *52*(3), pp.573-594.

[13] Dong, H. and Cui, L., 2015. System reliability under cascading failure models. *IEEE Transactions on Reliability*, *65*(2), pp.929-940.

[14] Peyghami, S., Wang, Z. and Blaabjerg, F., 2020. A guideline for reliability prediction in power electronic converters. *IEEE Transactions on Power Electronics*, *35*(10), pp.10958-10968.

[15] B. Zhang, M. Wang and W. Su, 2021. Reliability Analysis of Power Systems Integrated With High-Penetration of Power Converters. *IEEE Transactions on Power Systems*, vol. 36, no. 3, pp. 1998-2009.

[16] Dong, C., Zhao, Y. and Zhang, Q., 2016. Assessing the influence of an individual event in complex fault spreading network based on dynamic uncertain causality graph. *IEEE transactions on neural networks and learning systems*, *27*(8), pp.1615-1630.

[17] Saleh, M., Esa, Y. and Mohamed, A., 2018. Applications of complex network analysis in electric power systems. *Energies*, *11*(6), p.1381.

[18] Daemi, T., Ebrahimi, A. and Fotuhi-Firuzabad, M., 2012. Constructing the Bayesian network for components reliability importance ranking in composite power systems. *International Journal of Electrical Power & Energy Systems*, *43*(1), pp.474-480.

[19] Shi, Q., Liang, S., Fei, W., Shi, Y. and Shi, R., 2013. Study on Bayesian network parameters learning of power system component fault diagnosis based on particle swarm optimization. *Int. J. Smart Grid Clean Energy*, *2*(1), pp.132-137.

[20] Chen, X.W., Anantha, G. and Lin, X., 2008. Improving Bayesian network structure learning with mutual information-based node ordering in the K2 algorithm. *IEEE Transactions on Knowledge and Data Engineering*, *20*(5), pp.628-640.

[21] Tsamardinos, I., Brown, L.E. and Aliferis, C.F., 2006. The max-min hill-climbing Bayesian network structure learning algorithm. *Machine learning*, *65*(1), pp.31-78.

[22] Fu, L., He, Z.Y., Mai, R.K. and Bo, Z.Q., 2009, July. Approximate entropy and its application to fault detection and identification in power swing. In *2009 Power & Energy Society General Meeting* (pp. 1-8). IEEE.

[23] Namdari, A. and Li, Z., 2019. A review of entropy measures for uncertainty quantification of stochastic processes. *Advances in Mechanical Engineering*, *11*(6), p.1687814019857350.

[24] Schreiber, T., 2000. Measuring information transfer. *Physical review letters*, *85*(2), p.461.

[25] Kong, L., Pan, H., Li, X., Ma, S., Xu, Q. and Zhou, K., 2019. An information entropy-based modeling method for the measurement system. *Entropy*, *21*(7), p.691.

[26] Shannon, C.E., 2001. A mathematical theory of communication. *ACM SIGMOBILE mobilecomputing and communications review*, *5*(1), pp.3-55.

[27] Holmes, D.E. ed., 2008. *Innovations in Bayesian networks: theory and applications* (Vol. 156). Springer.

[28] Ankan, A. and Panda, A., 2015. pgmpy: Probabilistic graphical models using python. In *Proceedings of the 14th Python in Science Conference (SCIPY 2015). Citeseer* (Vol. 10).

[29] Faes, L., Nollo, G. and Porta, A., 2011. Information-based detection of nonlinear Granger causality in multivariate processes via a nonuniform embedding technique. *Physical Review E*, *83*(5), p.051112.

[30] Barrows, C., Bloom, A., Ehlen, A., Ikäheimo, J., Jorgenson, J., Krishnamurthy, D., Lau, J., McBennett, B., O'Connell, M., Preston, E. and Staid, A., 2019. The IEEE reliability test system: A proposed 2019 update. *IEEE Transactions on Power Systems*, *35*(1), pp.119-127.

[31] Grigg, C., Wong, P., Albrecht, P., Allan, R., Bhavaraju, M., Billinton, R., Chen, Q., Fong, C., Haddad, S., Kuruganty, S. and Li, W., 1999. The IEEE reliability test system-1996. *IEEE Transactions on power systems*, *14*(3), pp.1010-1020.

CHAPTER 5

Conclusions and Future Works

The main task of ongoing research is to explore the inter-relationship between power converters in terms of the system reliability impact, by utilizing Bayesian Network and Information Theory. This chapter briefly introduces the idea of ongoing research and summarizes future works.

In Chapter 2 and 3, we have investigated the reliability impact from device/converter to system level. However, whether a converter failure will affect other converter's reliability performance is still an unsolved puzzle. A failure happened on a power converter may result in an unsatisfactory load demand and the workload of adjacent converters would be increased accordingly. Therefore, there exists an inter-relationship between converters in terms of system reliability.

To graphically reveal the inter-dependencies between power converters, we will establish a directed acyclic graph (DAG) through Bayesian Network. In this DAG, each node represents a power converter, and each edge indicates the causality between two converters. Afterwards, the information entropy of each node (converter) is calculated to quantify the uncertainty level of each converter. Another information indicator from Information Theory named transfer entropy is estimated to determine the amount of information that each converter failure transferred.

Future works will focus on investigating the applications of parallel computing to speed up the proposed reliability analysis. The reliability impact of power converters' internal connections

in a RES is also worth investigating. The influence on the power system network changes (i.e., different network topologies) will change the power flow and ultimately affect the system reliability performance. Once the real-world or synthetic transmission networks become available for reliability analysis, one will be able to investigate the scalability of the proposed reliability assessment framework. Moreover, since ML encapsulates the relationship and acts like a 'black box', the integration of ML interpreting methods will be investigated to improve the reliability explanation and provide useful information for system operators. Appropriate reliability requirements on the converter level, and corresponding system maintenance strategies could be investigated.